Materials Today Bio 16 (2022) 100418

Contents lists available at ScienceDirect

Materials Today Bio

journal homepage: www.journals.elsevier.com/materials-today-bio

Smart nano-in-microparticles to tackle bacterial infections in skin tissue engineering

Marco Ruggeri [a], Barbara Vigani [a], Cinzia Boselli [a], Antonia Icaro Cornaglia [b], Daniele Colombo [a], Rita Sànchez-Espejo [c], Elena Del Favero [d], Narcisa Mandras [e], Janira Roana [e], Lorenza Cavallo [e], Laura Cantù [d], Cesar Viseras [c], Silvia Rossi [a], Giuseppina Sandri [a,*]

[a] Department of Drug Sciences, University of Pavia, Viale Taramelli 12, 27100, Pavia, Italy
[b] Department of Public Health, Experimental and Forensic Medicine, University of Pavia, via Forlanini 2, 27100, Pavia, Italy
[c] Department of Pharmacy and Pharmaceutical Technology, Faculty of Pharmacy, University of Granada, Campus of Cartuja S/n, Granada, 18071, Spain
[d] Department of Medical Biotechnology and Translational Medicine, University of Milano, LITA, Via Fratelli Cervi 93, 20090, Segrate, Milano, Italy
[e] Department of Public Health and Pediatric Sciences, University of Turin, 10126, Turin, Italy

ARTICLE INFO

Keywords:
Wound healing
Maltodextrin
Dextran
Amino acids
Metal oxide nanoparticles
Microparticles
Antimicrobial properties

ABSTRACT

Chronic wounds (resulting from underlying disease, metabolic disorders, infections, trauma, and even tumours) pose significant health problems. In this work, microparticles, based on polysaccharides (maltodextrin or dextran) and amino acids, and doped with antibacterial nanoparticles (CuO or ZnO NPs) are designed. Smart nano-in-microparticles with a hierarchical 3D structure are developed. The ultimate goal aims at an innovative platform to achieve skin repair and to manage skin colonization by avoiding infection that could delay and even impair the healing process. The microparticles are prepared by spray-drying and cross-linked by heating, to obtain insoluble scaffolds able to facilitate cell proliferation in the wound bed. The nano-in-microparticles are characterized using a multidisciplinary approach: chemico–physical properties (SEM, SEM-EDX, size distribution, swelling and degradation properties, structural characterization - FTIR, XRPD, SAXS – mechanical properties, surface zeta potential) and preclinical properties (in vitro biocompatibility and whole-blood clotting properties, release studies and antimicrobial properties, and in vivo safety and efficacy on murine burn/excisional wound model) were assessed. The hierarchical 3D nano-in microparticles demonstrate to promote skin tissue repair in a preclinical study, indicating that this platform deserves particular attention and further investigation will promote the prototypes translation to clinics.

1. Introduction

Wound healing is a complex process that involves coordinated interactions among different biological systems, including immune one, to restore the anatomical and functional integrity of skin [1,2]. Healing consists of different phases (haemostasis, inflammatory, proliferative and remodelling) and involves a complex series of events, such as chemotaxis, cell division, neovascularization, synthesis of the new extracellular matrix (ECM), and the formation and the remodelling of scar tissue. These events require multiple mediators, including platelets, inflammatory cells, cytokines, growth factors, and matrix metalloproteinases [3,4]. A cutaneous lesion causes the loss of the immunologic and protective mechanisms of the skin, so that microorganisms colonize the wounded area and occasionally lead to chronic infections and biofilm formation. In these cases, septicaemia can occur, and serious adverse life-threatening events can take place (such as amputations, organ loss and even death), if an adequate therapy is not effected [5,6]. For this reason, antimicrobial chemotherapy, specifically selected using antibiogram, is commonly recommend and systemic administration via parenteral or oral routes is required to reduce the risk of antibiotic resistance (AMR). In fact, AMR represents one of the greatest threats to human health, causing morbidity and mortality worldwide and high management cost-related [7]. A recent report estimated that infections by multidrug and drug-resistant bacteria caused in 2019 the death of 1.27 million people and if specific actions are not urgently taken, this number is projected to increase to ten million by 2050, thus overcoming the deaths caused by road accidents, diabetes, or cancer [8]. For this reasons, smart approaches to prevent and even treat wound infections should be

* Corresponding author.
E-mail address: g.sandri@unipv.it (G. Sandri).

https://doi.org/10.1016/j.mtbio.2022.100418
Received 29 June 2022; Received in revised form 31 August 2022; Accepted 2 September 2022
Available online 7 September 2022

implemented to tackle the development of resistant strains [9]. In this context, inorganic nanomaterials, including zinc oxide (ZnO) and copper oxide (CuO) proved to decrease or even eliminate antibiotic resistant bacteria, since they possess aspecific targets and act by disrupting the cell membranes, by causing protein misfolding, and by degrading cell key components such as DNA and proteins via oxidative stress [10].

Moreover, nanomaterials proved to play important roles in tissue adhesion, stem cell targeting, drug delivery, and differentiation and the synergy between physicochemical and biological (anti-microbial and angiogenesis) properties should trigger the successful design of alternative wound healing agents. However, the use of these metal-based nanomaterials as free nanoparticles poses significant limitations due to nanotoxicological issues while their immobilization in a 3D structure allows to achieve antimicrobial properties and simultaneously to avoid cytotoxicity, by enhancing the wound healing process [10].

To face the challenge of nanomaterials administration in this work the doping of inorganic nanomaterials in microparticles is proposed. An easily feasible and scalable method, the spray-drying, has been selected and the manufacturing has been designed as sustainable and green process. Moreover, the manufactured powder should allow a flexible dosing to cover and even fill a deep skin lesion. The resulting 3D structure should be able to control tissue moisture and to act as a scaffold to eventually enhance cell migration from the surrounding healthy tissue, cell adhesion and proliferation leading to the reconstruction of the architecture of native skin [11].

Given these premises, microparticles, based on polysaccharides (maltodextrin or dextran) and amino acids, and doped with antibacterial nanoparticles (CuO or ZnO NPs) were designed. Smart nano-in- microparticles with a hierarchical 3D structure were developed. The ultimate goal aimed at an innovative platform to achieve skin repair and to manage skin colonization by avoiding infection that could delay and even impair the healing process. Two different nanomaterials have been proposed on the basis of their properties, either CuO or ZnO NPs to identify the more suitable one to dope spray drying microparticles and to achieve wound healing and antimicrobial activity. ZnO and CuO proved antimicrobial activity against multi-drug resistant (MDR) strains [12,13]. The hierarchy of the systems has been achieved by the assembly of structures belonging to different length scales as microparticles and nanoparticles are.

The microparticles were prepared by spray-drying (SD) and cross-linked by heating to obtain insoluble scaffolds able to facilitate cell proliferation in the wound bed. Maltodextrin (MD) or dextran (DX), both are based on D-glucose units, were selected since they are of natural origin, in vivo degraded, biocompatible and non-immunogenic [14,15]. In particular MD is a linear glucan where glucose units are primarily linked with α(1 → 4) glycosidic bonds, while DX is a complex branched glucan, with the main chain consisting of α(1 → 6) glycosidic bonds between glucose monomers with branches from α(1 → 3).

MD or DX were associated to a mixture of threonine (Thr), cysteine (Cys) and glycine (Gly) (weight ratio Thr:Cys:Gly 1:2:10). This is a marketed association of amino acids present in topical antibiotics-based medicines (powder and cream) intended for the treatment of infected wounds (Cicatrene®, Johnson & Johnson SpA). Thr is a structural constituent of proteins and participates in the collagen and elastin formation and in the biosynthetic pathway of isoleucine [16]. Cys up-regulates metallothioneins and produces a specific inhibition of the collagenase activity of MMP. Together with glutamate and Gly, Cys participates in the synthesis of glutathione, one of the principal intra-cellular antioxidant systems [17]. Gly possesses anti-inflammatory properties acting through cell membrane hyperpolarization leading to decreased production of oxygen free radicals from inflammatory cells [18]. Moreover, it is a precursor of collagen and promotes the release of oxygen to the energy requiring cell-making process, which is essential for healing [19].

The nano-in-microparticles were characterized using a multidisciplinary approach: chemico–physical properties (SEM, SEM-EDX, size distribution, swelling and degradation properties, structural characterization - FTIR, XRPD, SAXS – mechanical properties, surface zeta potential) and preclinical properties (in vitro biocompatibility and whole-blood clotting properties, release studies and antimicrobial properties, and in vivo safety and efficacy on murine burn/excisional wound model) were assessed.

2. Materials and methods

2.1. Materials

MD (Glucidex 2, molecular mass: 8589 g/mol [20], degree of polymerization: 52.9, dextrose equivalent value: 2, Roquette, Giusto Faravelli, Milan, Italy) and DX (from *Leuconostoc mesenteroides* molecular weight ~200,000 Da, Sigma-Aldrich, Milan, Italy) were used as polysaccharides (Fig. S1). Gly, Cys and Thr (Sigma-Aldrich, Milan, Italy) were used as amino acids. Citric acid (CA, Sigma-Aldrich, Milan, Italy) was used as cross-linking agent. ZnO (Zinc oxide, dispersion nanoparticles, <100 nm particle size (TEM), ≤40 nm avg. part. Size, 20 wt % in H_2O, Sigma-Aldrich, Milan, Italy) and CuO NPs (Copper (II) oxide nanopowder, <50 nm particle size, Sigma-Aldrich, Milan, Italy) were used as inorganics.

2.2. Methods

2.2.1. Preparation of spray dried microparticles

SD (spray dried) microparticles were prepared using a mini spray drier (Buchi 190, Büchi Labortechnik AG, Essen, Germany) equipped with 0.5 mm nozzle. Polymeric blends were prepared (Fig. 1a reports the quali-quantitative compositions). Briefly, maltodextrin (MD) or dextran (DX) solution was obtained in distilled water and Thr, Cys and Gly at 1:2:10 wt ratio were added. Citric acid was added to the polymeric blends and used as cross-linker. The polymeric blends were sprayed as atomized droplets under 600 mL/h co-current feed air flow rate at 200 °C inlet air temperature (140 °C outlet air temperature) and immediately dried to obtain microparticles collected in the reservoir.

ZnO or CuO NPs doped microparticles were manufactured by adding NPs colloidal suspension to the initial polymeric blends before SD to have a 0.5% w/w concentration in the dried microparticles. The process yield was always higher than 50%. SD microparticles were then cross-linked by heating to activate citric acid (MD: at 140 °C for 2 h; DX: at 150 °C for 3 h).

2.2.2. Physico chemical characterizations

The microparticle morphology was assessed by SEM (Tescan, Mira3XMU, Brno, Czech Republic) before and after thermal treatment to activate the citric acid cross-linking. Samples were placed on metal stubs using a double-sided adhesive tape and sputtered with graphite under vacuum.

Moreover, the metal oxide NP doping was characterized by SEM-EDX (Phenom XL, Thermofisher, Alfatest, Cernosco sul Naviglio, Italy) of the section of the microparticles. Microparticles were crushed to obtain sections of the walls and EDX was performed in the wall thickness, then the samples were placed on metal stubs using a double-sided adhesive tape and sputtered with 5 nm gold under vacuum. The EDX spectra have been collected.

Particle size distribution was determined using DLS (dynamic light scattering) (Mastersizer 3000E granulometer, Malvern Instruments, Milan, Italy). Microparticles suspensions was prepared in isopropanol to avoid particle swelling. Particle diameters (D10, D50, D90) and distribution width (SPAN factor= (D90 – D10)/D50) were calculated.

2.2.3. Structural characterization

Fourier-transform infrared (FT-IR) analysis was performed using a JASCO 6200 (Tokyo, Japan) equipped with a Ge ATR. All analyses were performed from 400 to 4000 cm^{-1} with a resolution of 2 cm^{-1}, and the results processed with Spectra Manager v2 software.

a)

(% w/w)	MD	DX	Thr	Cys	Gly	Citric acid	ZnO NPs	CuO NPs
MD	5		0.125	0.25	1.25	1.25		
MD-ZnO	5		0.125	0.25	1.25	1.25	0.042	
MD-CuO	5		0.125	0.25	1.25	1.25		0.042
DX		5.97	0.125	0.25	1.25	1.25		
DX-ZnO		5.97	0.125	0.25	1.25	1.25	0.045	
DX-CuO		5.97	0.125	0.25	1.25	1.25		0.045

b)

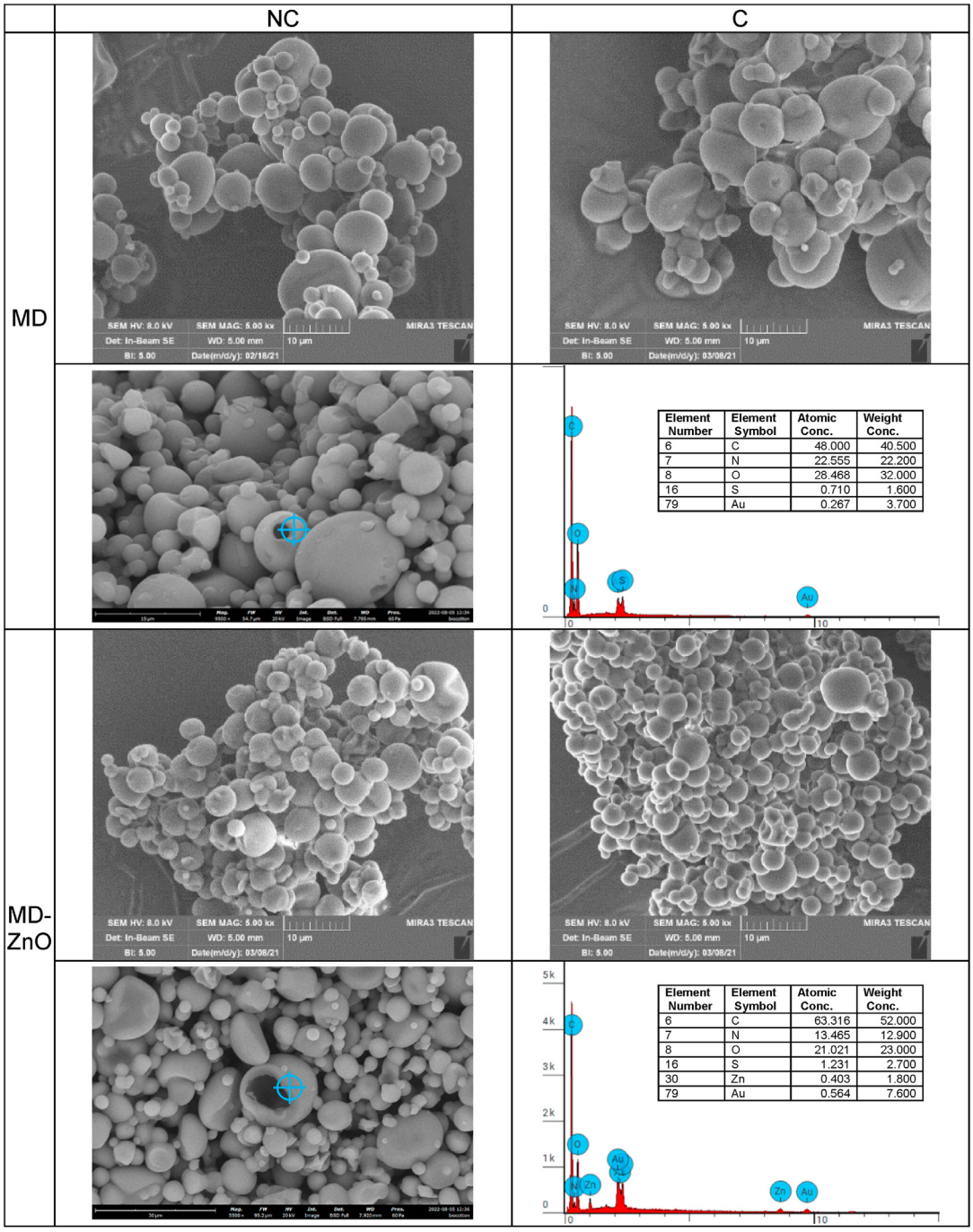

Fig. 1. a) Composition (% w/w) of polymeric blends used to prepare microparticles, b) SEM of the microparticles before and after cross-linking (top columns) and section of the microparticles and EDX analysis (bottom columns); c) Statistical particle diameters and SPAN factor (mean ± sd; n = 5) of microparticles before (nc) and after cross-linking (c). ANOVA one-way; Sheffé test ($p \leq 0.05$) D [4; 3]: MD nc vs MD c; MD-CuO nc vs MD-CuO c.

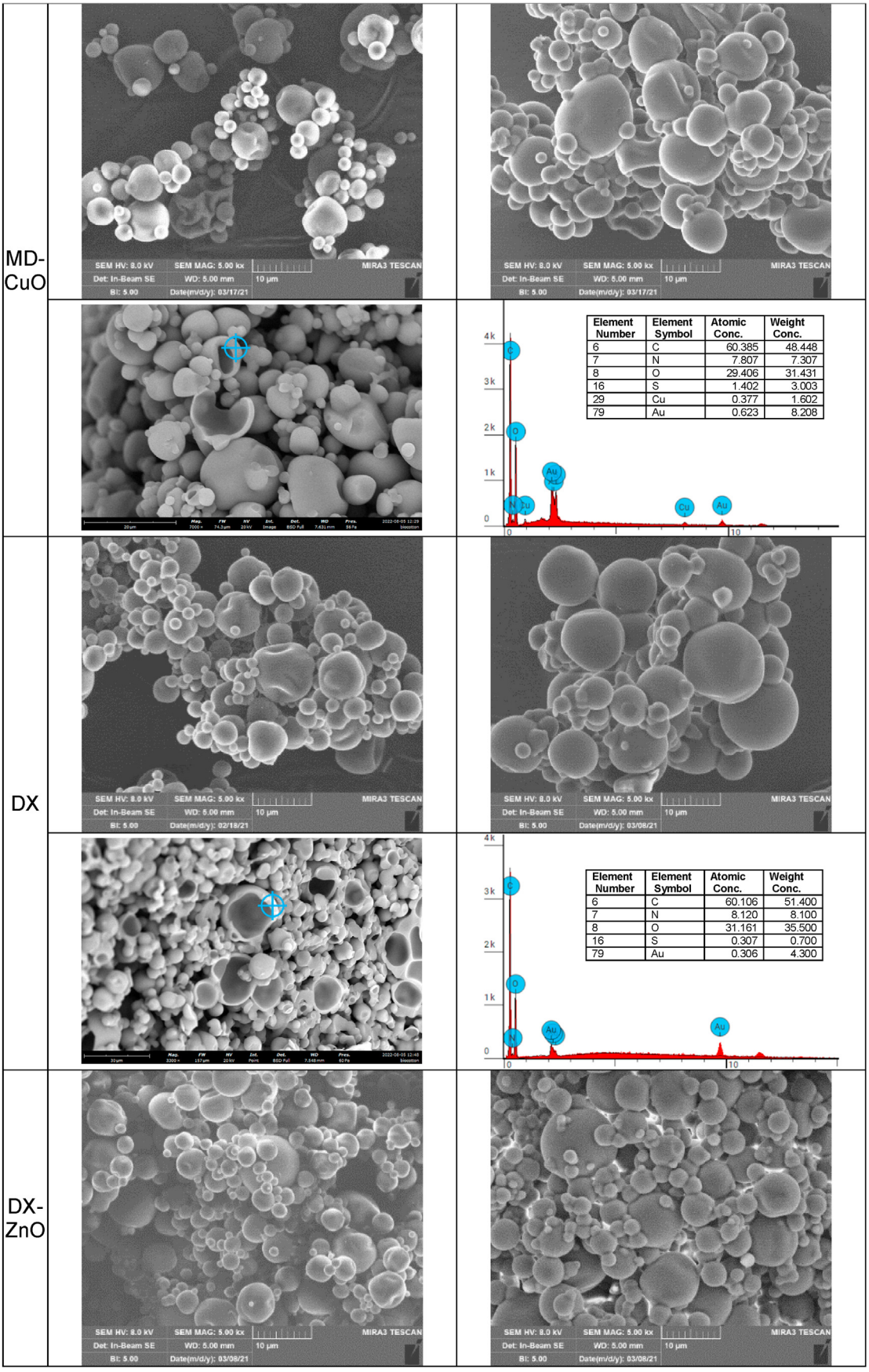

Fig. 1. (*continued*).

c)

Sample		d10 (μm)	d50 (μm)	d90 (μm)	d[4,3] (μm)	SPAN
MD	nc	6.3±0.2	14.9±0.6	38.7±1.8	19,2±0.7	2.2±0.1
	c	6.8±0.2	18.2±0.6	53.6±3.2	24.8±1.0	2.6±0.2
MD-ZnO	nc	5.7±0.2	16.2±0.4	52.5±1.7	23.4±0.6	2.9±0.1
	c	8.2±0.2	21.1±0.9	45.2±3.7	24.2±1.3	1.8±0.1
MD-CuO	nc	7.2±0.1	16.2±0.2	42.3±1.7	20.9±0.5	2.2±0.1
	c	8.9±0.1	22.4±0.5	46.7±2.9	25.4±1.1	1.7±0.1
DX	nc	8.1±0.3	19.8±1.2	39.5±3.4	22.0±1.5	1.6 ±0.1
	c	7.6±0.3	18.8±1.2	41.9±3.9	22.1±1.6	1.8±0.1
DX-ZnO	nc	8.5±0.2	21.8±1.0	49.1±4.2	25.6±1.7	1.9±0.1
	c	5.2±0.1	18.3±0.9	56.3±4.7	25.3±1.8	2.8±0.1
DX-CuO	nc	9.3±0.7	21.8±2.1	43.6±2.7	24.4±1.8	1.6±0.1
	c	6.4±0.2	17.9±0.6	54.2±1.0	26.1±0.5	2.7±0.1

Fig. 1. (*continued*).

Differential scanning calorimetry (DSC) and thermogravimetric analysis (TGA) were performed by means of a TGA/DSC1 equipment (Mettler-Toledo GMBH, Spain) equipped with a microbalance (precision 0.1 μg) and with a horizontal oven, in 25–950 °C temperature range and 10 °C/min heating rate, and in atmospheric air. Approximately 20 mg of each sample were weighted in aluminium sample pans.

Small Angle X-ray Scattering analysis was performed using synchrotron light at the ID02 SAXS beamline of ESRF (Grenoble, France). Dry microparticles were put in Kapton capillaries and fully hydrated with water. The scattered intensity was measured in $0.006 < q < 7.5\ nm^{-1}$ momentum transfer range, where $q = 4\pi sen(\theta/2)/\lambda$, being θ the scattering angle and $\lambda = 0.1$ nm the radiation wavelength. To this end, the intensity spectra were acquired at two different sample-to-detector distances, namely 1 m and 10 m, and joined after careful background subtraction. The intensity decays were fitted with models that describe the scattering from polymer chains in theta solvent or good solvent, following a random walk or a self-avoiding walk with SasView application [21], giving information on the mean radius of gyration R_g of the polymer chain on the local scale (nm length-scale), combined with a fractal arrangement on the mesoscale [22].

2.2.4. *In-vitro swelling and degradation measurements*

In-vitro swelling of the SD microparticles was evaluated by measuring the increase of particle diameters upon hydration. Microparticle suspensions were prepared in distilled water and gentle stirred for 24 or 48 h. Then the particle diameters were measured using DLS as previously described (paragraph 2.2.2). Swelling Index (SI) [23] was calculated as follows:

$$SI = (d[4:3]_t - d[4:3]_0) / \ d[4:3]_0.$$

where $d[4:3]_t$ is the volume weighted mean diameter at t time and $d[4:3]_0$ is the volume weighted mean diameter at time 0.

The in vitro degradation was assessed by incubating 20 mg/mL SD microparticles in phosphate buffer solution (PBS, pH 7.4, Sigma, Milan, Italy) at 37 °C. After 1, 2 and 7 days, SD microparticles were collected by centrifugation at 1000×*g* for 20 min at 4 °C. The supernatant was removed, the remaining particles were dried in an oven at 60 °C and the weight loss (%) calculated as the ratio between the weight after degradation and the initial weight [24]. After 48 h, the SD microparticle morphology was evaluated using SEM, as previously described (paragraph 2.2.3.).

2.2.5. *Particle crush test*

Particle crush test was performed on single particles having diameters ranging from 0.8 to 1 mm [25], using a texture analyzer (TA.XT plus, Stable Micro Systems, Godalming, UK) equipped with a 5 kg load cell and a P/10 probe (cylindrical, diameter = 10 mm). Before testing, an individual particle was placed on the base of the instrument. The probe was lowered at 10.00 mm/s speed, up to the particle crush and then pull back at 10.00 mm/s speed. The test was performed in the dry and wet state and the results were expressed as force of deformation (mN/mm), work of deformation (mN.mm) and Young Modulus (mN/mm^2).

2.2.6. *Surface zeta potential*

The apparent zeta potential (ζ) was assessed using SurPASS™ 3 (Anton Paar, Turin, Italy) equipped with a cylindrical cell. A fixed amount (50 mg) microparticles was placed between two paper filter disks in the cylindrical cell. 0.1 mol/L KCl solution was used as the streaming solvent and its pH was tuned in 2–9 range, to determine the ζ at physiological pH and the isoelectric point (iep) [2,26].

2.2.7. *Cell proliferation assay*

Proliferation and cell viability assay was carried out using fibroblasts (NHDF, normal human dermal fibroblasts from juvenile foreskin, PromoCell, WVR, Milan, Italy). Fibroblasts (2nd-5th passages) were cultured in Dulbecco's modified Eagle medium (DMEM, Sigma-Aldrich, Italy) supplemented with 10% fetal bovine serum (FBS, Euroclone, Milan, Italy), with 200 IU/mL penicillin/0.2 mg/mL streptomycin (Sigma-Aldrich, Milan, Italy), and kept at 37 °C in a 5% CO_2 atmosphere with 95% relative humidity (RH). Fibroblasts were seeded at $35*10^3$ cells/well density in 96-well plate and. After 24 h, each sample was dispersed in DMEM and put in contact with the cell substrates at different concentrations (10–0.5 mg/mL). Moreover, CuO or ZnO colloidal suspensions (containing the same metal oxide amounts as the microparticles) were also investigated. NHDF grown in standard conditions (growth medium, GM) was the control (100% vitality).

After 3 or 6 days of contact with the samples, the medium was removed and 50 μL MTT solution (3-[4,5-dimethylthiazole-2-yl]-2,5-diphenyltetrazolium bromide, Sigma-Aldrich, Italy) at 1 mg/mL in DMEM (w/o phenol red) were added for 3 h contact time. Subsequently, MTT solution was removed from each well, and the cell substrates were washed with 100 μL PBS. Finally, after PBS removal, 100 μL isopropanol (Sigma-Aldrich, Italy) were put in each well, and the absorbance was assayed at 570 nm by means of a microplate reader (FLUOstar® Omega, BMG LABTECH, Aylesbury, UK), with a reference wavelength of 690 nm. Cell viability was expressed as optical density (OD).

2.2.8. *Cell morphology*

The morphology of cells nuclei and cytoskeletons after 6 days of contact with the microparticles was investigated using CLSM after nuclei and cytoskeleton staining. 50 mg microparticles were placed into a 1 cm disc assembly unit and 2000 kg pressure were applied for 10 s to generate a disc with 0.6–0.8 mm thickness. These were placed on the bottom of a

well in a 48-wells/plate. NHDF (50×10^3 cells/well) were seeded onto microparticles discs and grown up to 6 days. The cells were fixed with 4% glutaraldehyde solution for 15 min and washed with PBS. Then, the cytoskeletons were stained with FITC Atto 488 phalloidin (50 μL at 20 μg/mL in PBS in each well, contact time 30 min) and the nuclei with Hoechst 33,258 (100 μL at 1:10.000 dilution in PBS per each well, contact time 10 min in the dark) (Sigma-Aldrich, Milan, Italy). Finally, the microparticles discs were mounted on glass slides, covered using coverslips and analyzed using CLSM (Leica TCS SP2, Leica Microsystems, Milan, Italy) at $\lambda_{ex} = 346$ nm and $\lambda_{em} = 460$ nm for Hoechst 33,258 and $\lambda_{ex} = 501$ nm and $\lambda_{em} = 523$ nm for FITC-phalloidin.

2.2.9. CuO/ZnO release

The release of Cu or Zn from nano-in-microparticles was evaluated. 20 mg microparticles were placed in 2 mL DMEM supplemented with 10% v/v FBS. The release experiments were performed at 37 °C and the inorganics were quantified over time (1, 6, 48, and 196 h). To avoid contaminations, no progressive sampling of the released medium was performed and independent tests using different time length were considered. The concentrations of Cu^{2+} and Zn^{2+} ions in the culture medium were measured using a NexION-300D ICP mass spectrometer (Perkin Elmer, Waltham, MA, USA), equipped with a triple cone interface and a quadrupole ion deflector using argon for plasma formation. Standard solutions were prepared for each element (Multi-Element standards, Perkin Elmer, Waltham, MA, USA), and Rh was employed as an internal standard.

2.3. Antimicrobial properties

The antibacterial activity of CuO or ZnO nano-in-microparticles were evaluated against *Escherichia coli* ATCC 8739 and *Staphyococcus aureus* ATCC 29213, a Gram-negative and Gram-positive bacteria, respectively. Tests were performed according to Clinical and Laboratory Standard Institute broth microdilution method [27]. CuO or ZnO NPs were serially diluted to obtain the final concentrations ranging from 0.03 to 15 mg/ml in a 96-well plate. These wells were then inoculated with bacteria (2×10^5 colony forming units, CFU/mL) supplemented with growth medium and the plates were kept for incubation at 37 °C for 18 h. Optical density (OD) at 600 nm was measured. MIC (minimum inhibitory concentration) and MBC (minimum bactericidal concentration) were obtained to assess antibacterial activity. MIC is the lowest concentration inhibiting the visible growth of bacteria after 18 h of incubation. MBC is the lowest concentration of the sample (mg/mL) that kills 99.9% (3 log) of the bacteria tested.

As for time kill curve assay, the inocula were prepared according to CLSI guidelines for studying time kill kinetics. Briefly, *E. coli* ATCC 8739/*S. aureus* ATCC 29213 cultures, in exponential phase, were adjusted to 1×10^7 CFU/mL in BHI medium and split into eight 500 μL aliquots. Aliquots were inoculated with 500 μL containing 0.5 mg/mL of 2 days release samples. These were incubated at 37 °C for 2, 4, 24, 48 h. At different times, bacterial growth was evaluated by the serial dilution technique and the spread of samples on top of TSA plates. The microbiocidal effect (ME value) was calculated for each test organisms and contact times according to the following equation:

$$ME = \log N_c - \log N_d$$

where N_c is the number of CFU of the control microbial suspension and N_d is the number of CFU of the microbial suspension in presence of the scaffold.

CFUs were counted and compared with the control: a 3 log decrease in the viable counts indicated bactericidal activity of sample.

2.3.1. In vitro whole-blood clotting

The haemostatic activity of microparticles was evaluated using rat whole bloods pooled from 6 male rats (Wistar 200–250 g). All animal experiments were carried out in full compliance with the standard international ethical guidelines (European Communities Council Directive 86/609/EEC) and approved by Italian Health Ministry (D.L. 116/92). The whole blood pool was supplemented with 10% v/v of acid-citrate-dextrose (ACDC, 38 mM citric acid/75 mM trisodum citrate/100 mM dextrose) to avoid the coagulation during the storage at 4 °C [28]. Just before the experiments, the anticoagulant activity of ACDC was inhibited by diluting 200 μL blood with 200 μL saturated $CaCl_2$ solution, then 25 mg microparticles were added and incubated for 3 min. As for haemoglobin absorbance quantification, after 3 min contact, 1 mL distilled water was added and gently shaken for 2 min to re-suspend free red blood cells, not entrapped in the clot. The absorbance of each sample was assayed by means of spectrophotometric detection at λ 542 nm (Lamba25, Perkin Elmer, Milan, Italy). Fresh blood was considered as reference.

As for the SEM analysis, the blood was fixed with 3% glutaraldehyde (Sigma-Aldrich, Milan, Italy) for 1 day. After washing with PBS, dehydration was performed by immersing blood in 50%, 75%, and 100% ethanol, and the blood clots were observed by SEM.

2.3.2. In vivo systems safety and efficacy

All animal experiments were carried out in full compliance with the standard international ethical guidelines (European Communities Council Directive 86/609/EEC) approved by Italian Health Ministry (D.L. 116/92). The study protocol was approved by the Local Institutional Ethics Committee of the University of Pavia for the use of animals and by ISS (Istituto Superiore di Sanità). 9 male rats (Wistar 200–250 g, Envigo RMS S. r.l.) were anesthetized with equitensine at 3 ml/kg (39 mM pentobarbital, 256 mM chloral hydrate, 86 mM MgSO4, 10% v/v ethanol, and 39.6% v/v propylene glycol) and shaved to remove all hair from their backs. All animals were then carefully monitored for the following 3 days by animal care services and received additional treatment of the same pharmacological treatments.

Microparticles were subcutaneously implanted by means of an 8 mm incision (one for each rat) in the rat back. The incisions were then sutured using strips (Steri-Strip Suture, I). 18 days after the treatment, full thickness biopsies were taken in correspondence of the incisions and the histological analysis was performed. A biopsy of intact skin was also taken for comparison.

Three circular full thickness burns, 4 mm in diameter, were produced on the back of the animals by means of the contact with an aluminum rod (105 °C for 40 s). 24 h later, the formed blisters were removed using a 4 mm diameter biopsy punch to obtain a full-thickness lesions. 20 mg of microparticles were applied and wetted with 20 μl of saline solution (0.9 g/L). Lesions treated with 20 μL of saline solution were the negative control. Lesions were covered with a sterile gauze and the rat back was wrapped with a surgery stretch (Safety, Italy) to protect lesions. At prefixed times after blister removal (0, 3, 7, 10, 14 and 18 days) photographs of the lesions were taken by using a digital camera (Sigma SD 14) which allowed for sizing the lesions and monitoring the healing process. The size of wounded area was determined with an image analysis software (Image J, ICY, Institute Pasteur, France). 18 days after the treatment, full thickness biopsies were taken in correspondence of the initial lesions and the histological analysis of the excised tissues was performed. A biopsy of intact skin was also taken for comparison.

Moreover , the area around the scar or residual wound was harvested and wound tissue specimens (wound bed) were immediately immersed in the fixative solution (4% neutral buffered formaldehyde), embedded in paraffin and sectioned at a thickness of 5 μm. Sections were stained with either hematoxylin and eosin (H&E), or with picrosirius red (PSR). As for Picrosirius red staining, deparaffinized sections were hydrated, faintly stained with Weigert's hematoxylin for nuclei, and stained with PSR (1 h). Then all sections were dehydrated, cleared in xylene and mounted with DPX.

Stained sections were observed with a light microscope Carl Zeiss Axiophot provided for circular polarizing microscopy, with suitable

filters in the condenser stage and in the microscope tube. Images were recorded through a microscope digital 5 megapixels CCD camera Nikon DS - Fi2.

2.3.3. Statistical analysis

Statistical analyses were performed using Astatsa statistical calculator. One-way analysis of variance (ANOVA) was followed by Scheffé for post-hoc comparisons. $p < 0.05$ was considered significant.

3. Results and discussion

3.1. Chemico-physical properties

Fig. S2 reports the TEM micrographs (left) and the size distribution of the ZnO and CuO NPs (right). The nanoparticles are characterized by a regular size and a slight tendency to aggregation. In particular, CuO NPs are characterized by a rod shape while ZnO NPs have spherical ones. ZnO NPs show a mean diameter lower than 40 nm while CuO NPs lower than 50 nm. Moreover, NPs have mild polydispersion ($0.24 \pm 0.02 \leq PDI \leq 0.27 \pm 0.01$) with negative zeta potentials, and specifically -18.25 mV or -30.33 mV for CuO or ZnO, respectively.

Fig. 1b shows the SEM micrographs of SD nano-in-microparticles (top columns) and section of the microparticles and EDX analysis (bottom columns).

Independently of the composition, the SEM images show heterogeneous microparticles with a smooth surface and a predominantly spherical shape, although some have a spheroidal appearance, as reported in literature for most of the spray-dried formulations [29]. The NP doping does not alter the microparticles morphology. The cross-linking of the microparticles by heating treatment allows to obtain insoluble substrates in aqueous environment without loss of structural integrity and morphology. In the microparticles, the Zn^{2+} and Cu^{2+} doping is evident from the elemental compositions (SEM-EDX) (Fig. 1b): the microparticles sections show that the particles are characterized by inner voids and that Zn^{2+} and Cu^{2} are present in the polymeric matrix of the microparticles walls (Fig. S4 reports the composition in Zn or Cu as determined with EDX in different points of the microparticle section). Nano-in-microparticles morphology is mainly attributable to the manufacturing process rather than to the systems composition, indicating that MD or DX do not have impact on the system development.

Fig. 1c reports the particle diameters and SPAN factor of microparticles before (nc) and after cross-linking (c). All the SD microparticles show a narrow particle size distribution with a mean diameter (D[4; 3]) between 19 and 26 μm. Moreover, the particle size is slightly greater for the ZnO or CuO NPs doped microparticles.

MD-based microparticles are smaller than those based on DX and this should be directly related to the chemico-physical properties of the polymer blend used for microparticles manufacturing: MD-based blends are characterized by surface tension and viscosity (as reported in SI, Table S1 and Fig. S3) lower than those based on DX and this could lead to smaller drops during spray drying, resulting in the formation of fine particles.

The cross-linking affects particle size and in particular, the CuO NP or ZnO NP doped MD-based microparticles show a size increase of about 30% or 20%, respectively, upon cross-linking, although all the doped or undoped microparticles are characterized by similar dimensions. This is not evident in DX based systems which have similar dimensions independently on doping and cross-linking. MD, characterized by linear structure, seems more sensitive to cross-linking than DX, having a branched conformation: the heating process is conceivably able to favour the formation of cross-links in a linear structure, more flexible and prone to interdiffusion into a polymer matrix, rather than a rigid branched structure characterized by steric hindrance.

Fig. 2a reports the FTIR profiles of the microparticles before and after cross-linking. Independently of CuO or ZnO doping, cross-linking causes a significative effect in the region around 1640 cm^{-1}, typical of the Amide I band. This could be related to the formation of covalent bonds occurring between amino acids amino groups and carboxylic moieties of citric acid, caused by the heating treatment. However, the doping does not significantly influence the cross-linking process probably also due to the low content of ZnO or CuO NPs in the microparticles.

Fig. 2b reports the thermal analysis of the microparticles before and after cross-linking process (TGA - top panel, DSC - bottom panel).

The thermal behaviour of the pristine components is reported in Figures S5 (TGA) and S6 (DSC). Both MD and DX show a weight loss in three stages with total carbonization at 500 °C or 550 °C, respectively. MD and DX thermal degradation profiles show a first small weight loss at around 95 °C due to the water evaporation (7.8% and 7.7% weight loss, respectively) followed by an intense weight loss (71.6% and 71.9%, respectively) at around 300 °C, corresponding to MD or DX depolymerization and finally the continuous degradation of resultant residues at about 490 °C. Citric acid also showed an intense weight loss at 220 °C followed degradation of resultant residues up to 400 °C. Gly, Thr and Cys are characterized by no weight loss up to 220–250 °C, and a second stage of weight loss closed at 500/600 °C.

All the microparticles (Fig. 2b – top panel) show a first water loss followed by a two-stages degradation at temperature higher than 200 °C. In general, independently of the composition, the not cross-linked microparticles show, at temperatures higher than the cross-linking ones (see insets in Fig. 2b), a more intense and fast degradation stage compared to cross-linked microparticles, suggesting that the cross-linking increases the stability to thermal degradation.

Parallelly, MD and DX do not show any endothermic peak, while amino acids profiles showed intense melting peaks at temperature higher than 200 °C, indicating that the pristine materials are crystalline. The microparticles (Fig. 2b – bottom panel) show a first broad peak (30–130 °C) corresponding to the water evaporation. At temperature higher than 160 °C other endothermic peaks are present corresponding to the component degradation. This thermal behaviour supports the microparticles stability upon the cross-linking by heating. Moreover, the cross-linking seems to further stabilize the systems at higher temperatures, causing systems degradation at temperature slightly higher than the not cross-linked systems.

The small angle x-ray scattering (SAXS) spectra of microparticles are reported in Fig. 2c. The inner structure of undoped microparticles in wet conditions suggests that MD-based microparticles differently behave from DX ones. In particular, the polymer local arrangement, on the scale of lengths between nm and hundreds of nm in identical wet conditions in aqueous dispersion, is dramatically influenced by the cross-linking.

The scattered intensity profiles are different for MD-based and DX-based microparticles. The spectra of not cross-linked systems show the polymers arrangement in aqueous dispersion (lower experimental points in both panels) (Fig. 2c, upper panels).

The MD intensity profile is fitted (green line) with a gaussian coil model that describes the scattering from polymer chains in theta solvent, where the polymer arranges following a random walk, curling up on coils with characteristic size (radius of gyration, Rg) and structure. The mean Rg is 9 nm.

DX intensity profile displays different features. In the high-q region, corresponding to the local arrangement of polymer chains, the intensity profile is fitted with a model for polymer chains subject to excluded volume effects in good solvent, where the polymer arranges following a self-avoiding walk, curling up on coils with characteristic Rg of 5 nm. At low q values ($q < 0.03$ nm^{-1}) the experimental points deviate from this behaviour, indicating an additional different internal arrangement of polymers on a longer length-scale. The intensity follows a $I(q) \div q^{-2.7}$ decay, suggesting a loose DX packing on the hundreds of nm length scale. The observed different arrangement of DX chains agrees with their branched structure.

After cross-linking, the characteristic Rg of both polymers in aqueous

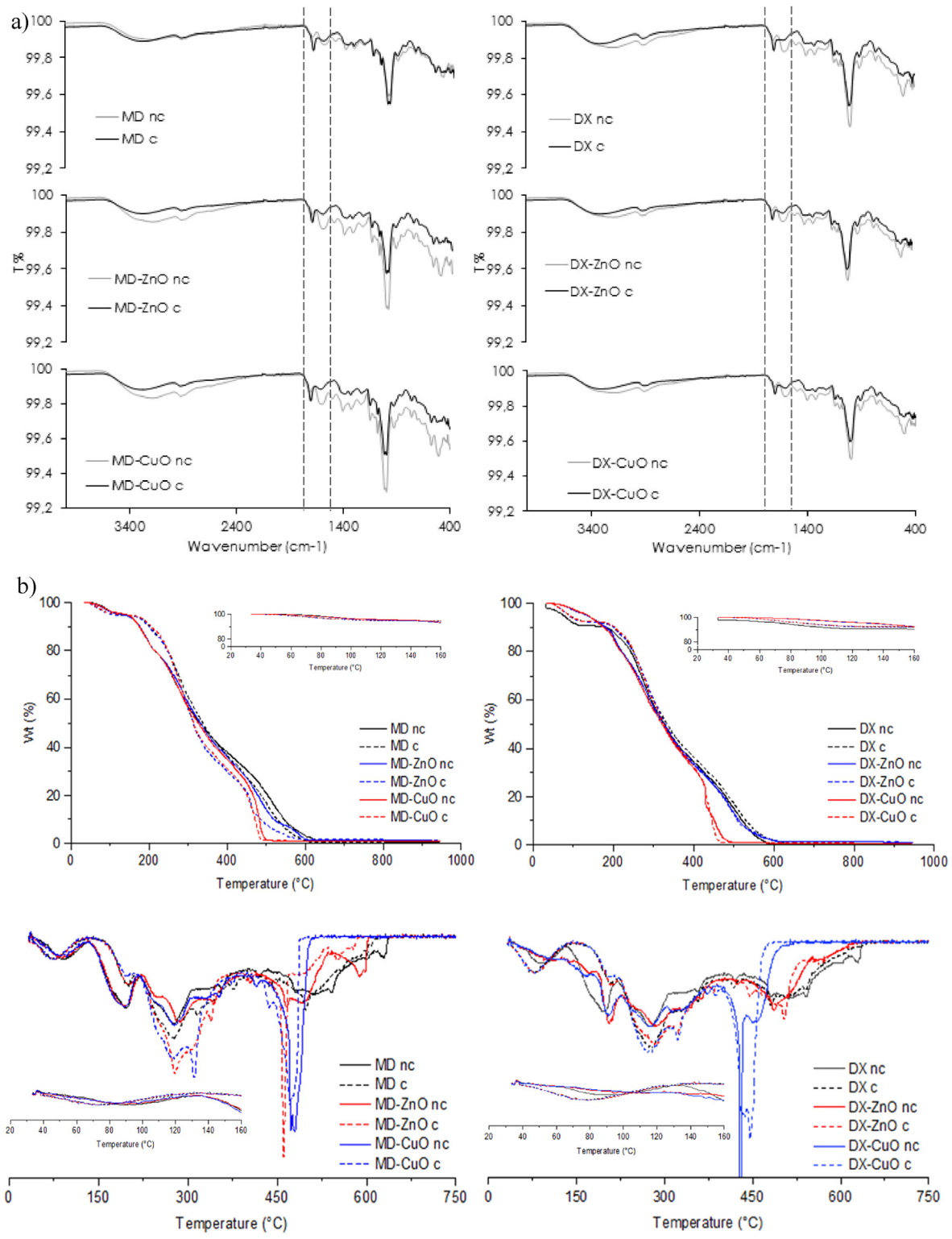

Fig. 2. a) FTIR spectra of the microparticles after and before cross-linking, b) Thermal analysis (TGA and DSC) of not cross-linked (nc) and cross-linked (c) microparticles, c) small angle x-ray scattering (SAXS) spectra of not cross-linked and cross-linked microparticles in fully wet condition and of doped microparticles (lines are the fitting curves).

dispersion decreases down to about 2 nm. On the local scale, the inner structure of cross-linked microparticles is characterized by the entanglement of polymers on the length of few nms.

At low q values, both experimental spectra assume a steep decay, $I(q) \div q^{-2.7}$ for DX, and $I(q) \div q^{-4}$ for MD. These results indicate a different density of the two systems on the hundreds of nanometers length-scale, being the MD able to realize close-packed structures, while DX keeps a looser packing, as observed in the not cross-linked system.

The addition of ZnO and CuO NPs affects the internal structure of cross-linked microparticles on both the local and the hundreds of nm

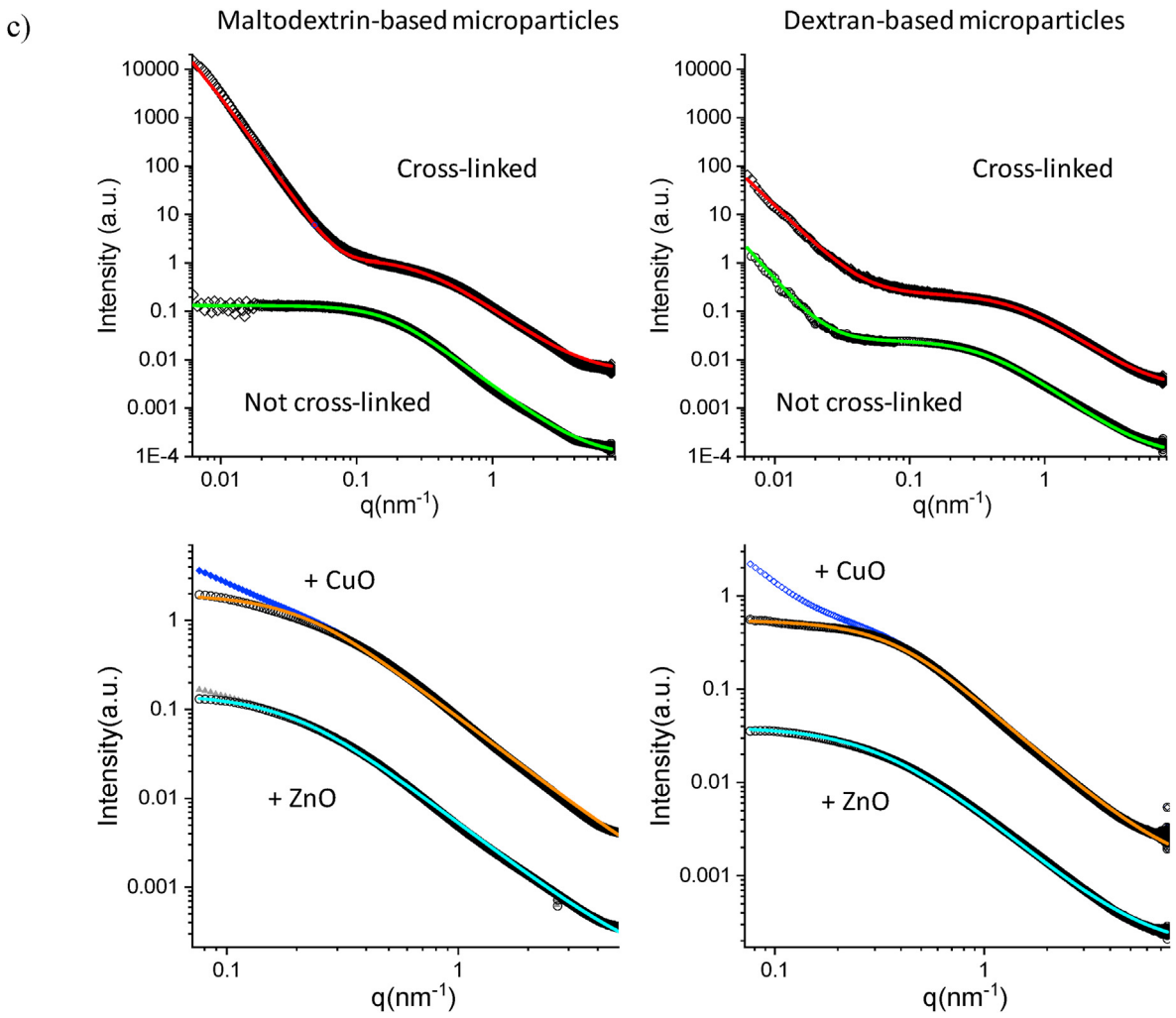

Fig. 2. (*continued*).

length-scale, as visible in the small angle x-ray scattering (SAXS) spectra measured for doped MD and DX microparticles (in SI, Fig. S7). Fig. 2c (bottom panels) reports the high-q region of the spectra. The intensity decays are fitted with a Gaussian coil model after subtraction of the contribution of the ZnO or CuO NPs (in SI, Fig. S8). The characteristic sizes become slightly larger for all systems, for MD Rg = 8 nm (ZnO) and Rg = 7 nm (CuO), while for DX Rg = 5 nm (ZnO) and Rg = 4 nm (CuO). The intensity decays in the low-q region are reported in Fig. S8. The scattered intensity of doped microparticles assume a less steep decay with respect to the undoped ones, $I(q) \div q^{-2.5}$ for DX-CuO, and $I(q) \div q^{-3.4}$ for MD-CuO and MD-ZnO. Overall, results indicate a looser internal packing of doped microparticles on the hundreds of nm length-scale, especially noticeable for maltodextrin-based microparticles. These changes in the internal structure indicate nanoparticles in microparticles arrangement with CuO NP or ZnO NP embedded in the polymer matrix and that those NP are homogeneously distributed in the polymer matrix of the microparticles.

3.2. In-vitro swelling and degradation properties

Hydration behaviour is crucial since this should favour haemostasis and guarantee a balance between the exudate absorption and the wound bed dehydration, both essential features in the granulation phase [24]. Fig. 3a reports the swelling properties after 24 and 48 h, expressed as swelling index. DX-based microparticles swell more than MD-based microparticles and this is agreement with the cross-linking effect and the structural analysis. The doping seems to reduce the microparticles swelling and this is a consequence of the NPs role in the structure to enhance packed systems: the NPs could act as assembly point taking the polymer chains closer each other and less mobile, thus reducing the swelling process.

Fig. 3b shows the degradation behaviour (weight loss expressed as weight residue) of microparticles versus time in PBS at 37 °C. DX-based microparticles show a marked effect of weight loss, suggesting a degradation rate faster than that of MD-based microparticles after 1 and 2 days of incubation. Moreover, after 7 days, the residues of MD based systems range from 36% (ZnO doping) to 48% (no doping) while for DX they range from 31% (ZnO doping) to 35% (no doping), although those are not significantly different. The degradation profiles are conceivably linear, and this suggests a complete degradation within 10 days. After 48 h, SEM images the microparticles rougher and partially fused to form conglomerates. The highest the packaging of the polymer matrix to form microparticles (as for MD) the slowest the degradation rate.

3.3. Mechanical properties

Fig. 4 shows the mechanical properties of the microparticles (deformation force mN/mm - a,d; deformation work mN.mm – b,e; Young Modulus mN/mm^2 – c,f) in the dry (a-c) or wet (d-f) state.

The doped microparticles appear less elastic than the undoped ones,

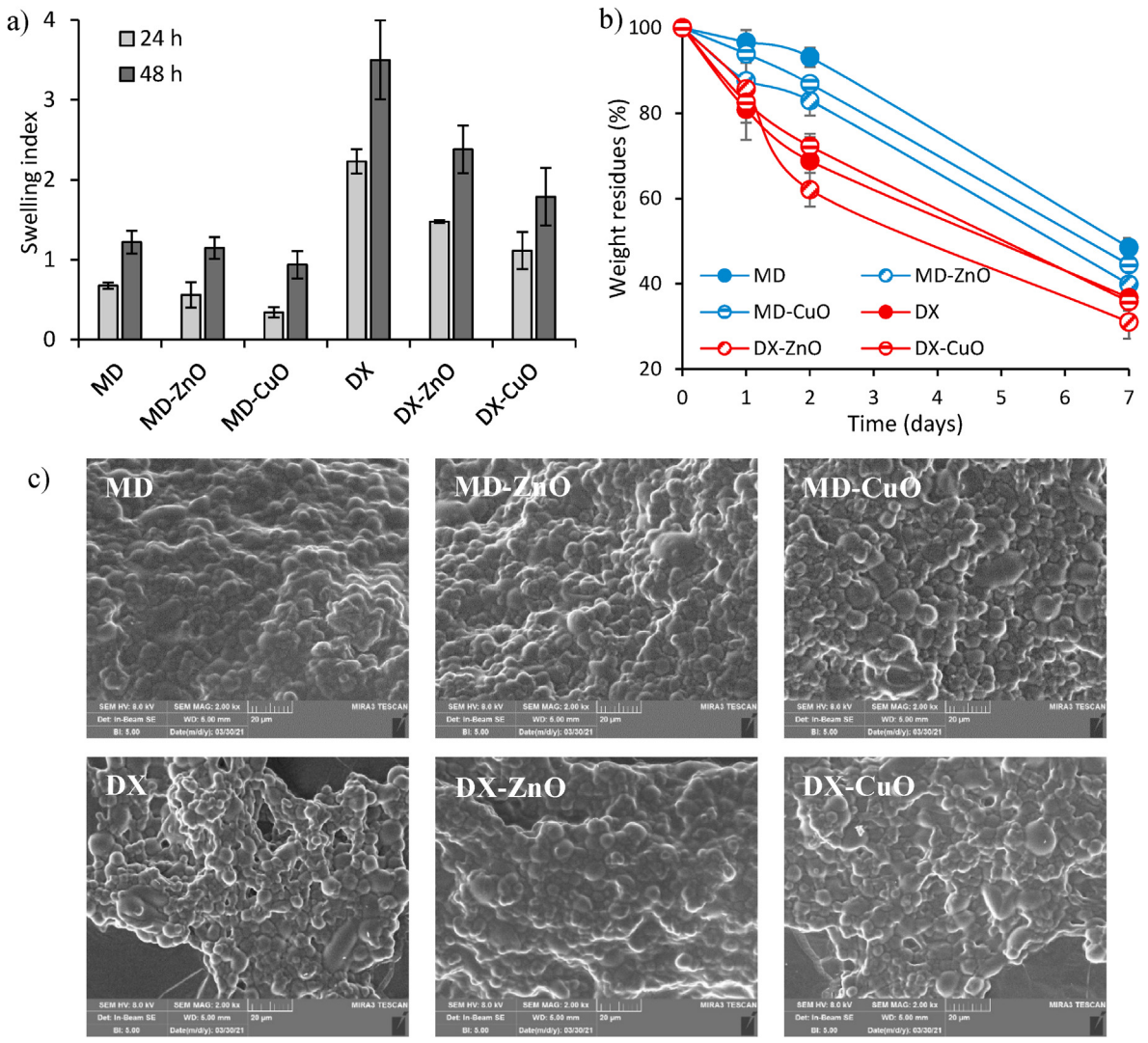

Fig. 3. a) Swelling properties of spray-dried microspheres expressed as Swelling Index and b) weight residues of spray-dried microspheres after 24 and 48 h incubation in PBS at 37 °C; c) SEM images of spray-dried microparticles after 48 h of incubation in PBS at 37 °C. ANOVA one-way; Sheffé test ($p \leq 0.05$): Fig. a) MD 24 h vs MD 48 h, MD-ZnO 24 h vs MD-ZnO 48 h, MD-CuO 24 h vs MD-CuO 48 h, DX 24 h vs DX 48 h, DX-ZnO 24 h vs DX-ZnO 48 h, MD-CuO 24 h vs MD-CuO 48 h; Fig. b) MD-ZnO 24 h vs MD-ZnO 48 h, DX 24 h vs DX 48 h, DX-ZnO 24 h vs DX-ZnO 48 h, MD-CuO 24 h vs MD-CuO 48 h.

while no significant differences on the deformation forces are observed.

The mechanical properties are dramatically influenced by hydration. At the dry state, the undoped microparticles are characterized by higher deformation force and elasticity. On the other hand, following hydration, the breaking force, the deformation work, and the Young's modulus significantly decrease. NPs embedded in the polymer matrix act as wrapping point and could interrupt the polymer chains entanglements: this modifies the microparticle structure decreasing the elasticity. In particular, the NPs doping, especially for the hydrated systems, seems to render the microparticles structure highly deformable and adaptable to the application site.

3.4. Surface zeta potential

Fig. 4 g-l show the zeta potential (mV) values as a function of pH. The microparticles show a negative zeta potential at physiological pH (pH 7), due to the presence of citric acid. Moreover, ZnO and CuO NPs doping lowers the zeta potential profiles.

MD-based microparticles have isoelectric points (iep) higher that DX based ones: this means that the systems have different behaviour at the solid-liquid interface.

3.5. Biocompatibility and cell morphology

Fig. 5a shows the fibroblasts viability (OD - optical density) after 3 and 6 days of incubation.

The microparticles properties are compared to the ZnO and CuO NPs at the same concentrations equal to those of the doped microparticles and with a standard growth condition (GM - growth medium). The GM suggests that cell population increases from 3 to 6 days, and this is evident also for the samples, indicating that microparticles are able to support cell growth along time without impairing their proliferation. Doped MD or DX-based microparticles are characterized by a performance significantly better than that of ZnO or CuO NPs. This means that the microparticles are able to protect the cells, suggesting that they are able to avoid the cytotoxicity of the metal oxides. This could be due to the ability of the microparticles to control the ions release and the ability of the formulations to favour the proliferation of fibroblasts.

Fig. 5b reports the CLSM micrographs of fibroblasts grown for 6 days onto the microparticles. Fibroblasts are able to adhere, to grow and to spread all over the microparticles, maintaining their fusiform structure with cytoskeletons formed of elongated filaments.

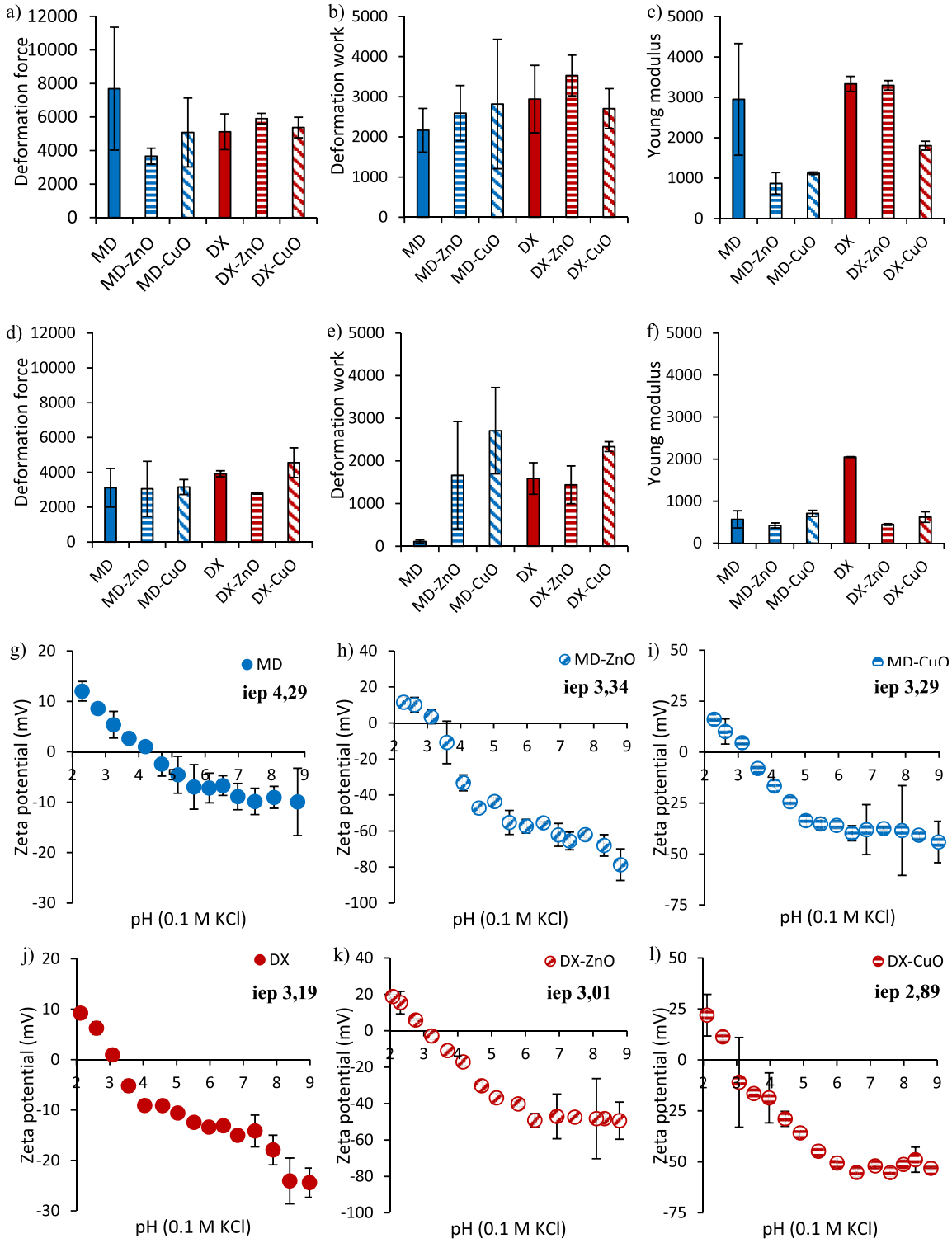

Fig. 4. Mechanical properties (a,d deformation force mN/mm; b,e deformation work mN.mm; c,f Young Modulus mN/mm^2) in the dry (a–c) or wet (d–f) state (mean values ± sd; n = 3). ANOVA one-way; Scheffé's test ($p \leq 0.05$): a) MD vs. MD-ZnO; c) MD vs. MD-ZnO, MD-CuO, DX-CuO; DX vs DX-CuO; DX-ZnO vs. DX-CuO; e) MD vs. MD-ZnO, MD-CuO, DX, DX-ZnO, DX-CuO; MD-ZnO vs MD-CuO; f) DX vs. MD, MD-ZnO, MD-CuO, DX-ZnO, DX-CuO. Zeta potential profiles vs pH of MD (g) MD-ZnO (h), MD-CuO (i), DX (j) DX-ZnO (k), DX-CuO (l) (mean values ± s.d.; n = 3).

3.6. Ions release measurements

Fig. 6a reports zinc and copper (%) released vs time. Independently of the type of polymer, zinc profiles reach quantitative release within 6 h, while copper is slowly released. These behaviours seem related to the particle size of ZnO or CuO NPs and to the type of polymeric matrix. It is conceivable that zinc is readily available thanks to ZnO nanoparticles dimensions (smaller) that allow their escape from polymer network and to their higher surface area that allows greater ion exchange with the environmental medium. On the other hand, copper seems less prone to have a prompt release and this seems much more dependent to the polymeric matrix composition: in fact, maltodextrin heavily affects

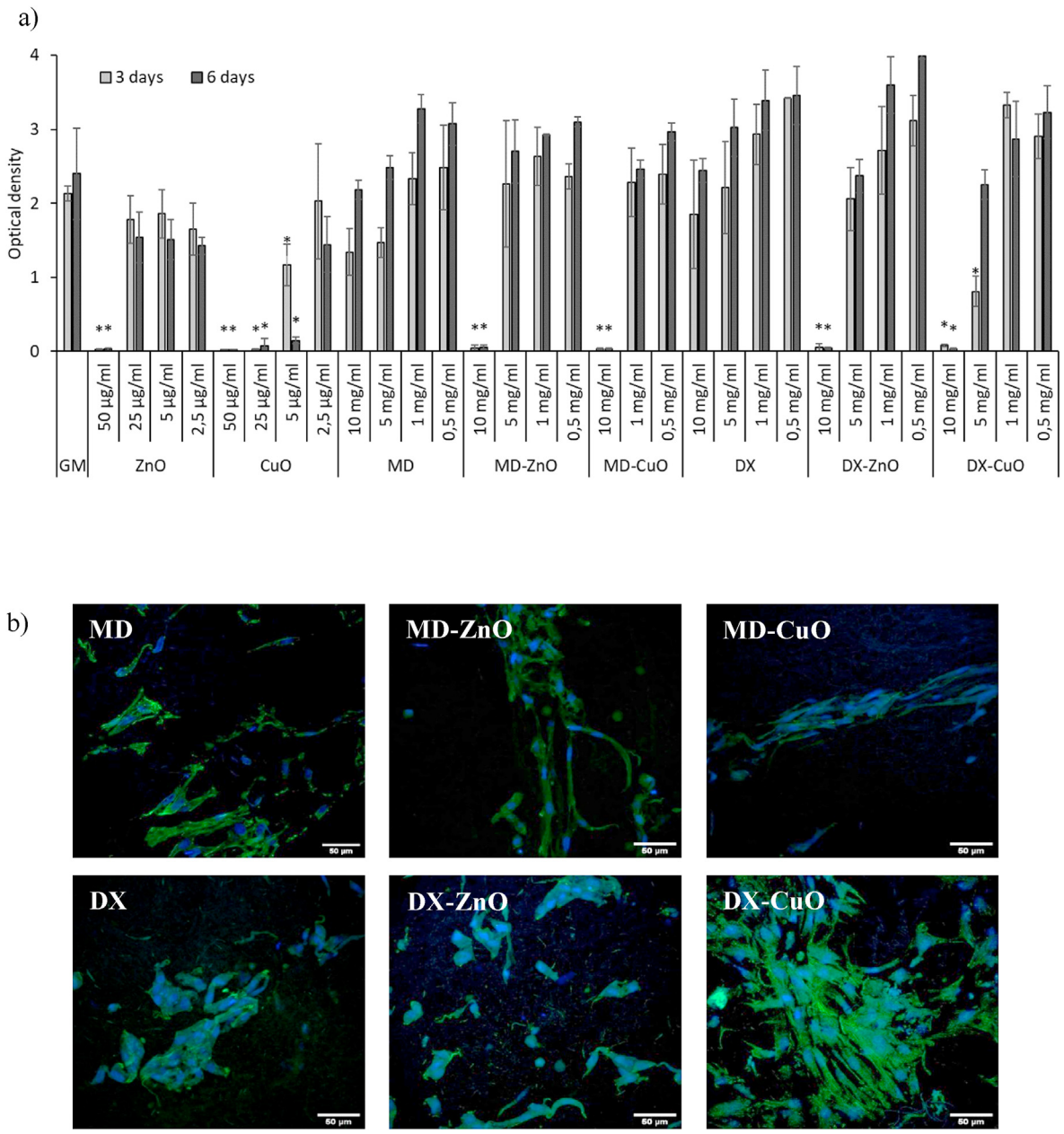

Fig. 5. Viability (optical density) of fibroblasts after 3 days and 6 days (a) of contact with CuO and ZnO NPs as suspension, and with microparticles (MD, MD-CuO, MD-ZnO, DX, DX-CuO, DX-ZnO) in comparison to the positive control GM (growth medium, as standard growth conditions) (mean values ± s.d.; n = 5). Values * are statistically significant ($p \leq 0.05$) compared with control. Confocal laser scanning microscopy (CLSM) micrographs (b) of fibroblasts grown for 6 days onto microparticles (in blue: nuclei; in green: cytoskeletons) (scale bar: 50 µm).

copper release, and this seems mainly caused by higher chain entanglement of the polymer chains wrapped onto NPs and less hydration and swelling properties that impair inorganic nanoparticles to diffuse.

3.7. Antimicrobial properties

The antimicrobial test aims at verifying the retention of the establish antimicrobial activity [12] upon loading into the microparticles. For this reason, two representative strains, a Gram positive and a Gram negative, *S. Aureus* and *E. coli*, respectively, have been considered.

Fig. 6b reports MIC/MBC. Independently of the polymer type (MD or DX) and the doping (CuO or ZnO), the systems appear to be more effective against Gram positive rather than Gram negative (MIC = 7.5 mg/ml vs MIC = 15 mg/ml, respectively). Although the MBC/MIC ratios (bactericidal capacity) are lower than 4 suggesting negligible bactericidal properties in all cases, the time kill assay (Fig. 7 c) shows that the samples obtained from the release experiments possess a certain antimicrobial activity against *E. coli* ATCC 8739 and mainly against *S. aureus* ATCC 29213. Time-kill kinetics suggest a significant decrease of viable *S. aureus* cells after 2 h contact time of ZnO-MD microparticles: this is coherent with previous study by Steffy et al., 2018 [30]. Similarly, CuO-DX microparticles show a bactericidal effect in the first 2–4 h, however, viable bacteria increase upon longer contact time suggesting a decrease of bactericidal effect for prolonged time. These results are supported by previous findings that state ZnO nanoparticles are much more effective as antibacterial agent against Gram-positive bacteria than Gram-negative ones [30].

On the contrary, CuO-MD microparticles are mainly effective against *E. coli* showing a reduction of bacterial load in the different incubation times. This agrees with the study by Rajamma et al. [31]. The mechanism

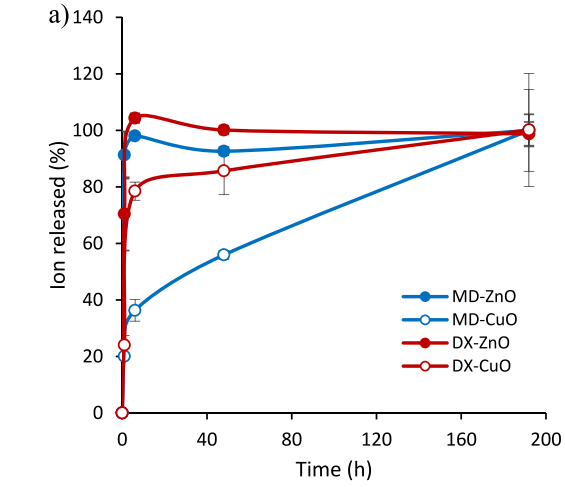

b)

	E. Coli		S. aureus	
	MIC	MBC	MIC	MBC
MD	15	15	7.5	7.5
MD-ZnO	15	15	7.5	15
MD-CuO	15	15	7.5	15
DX	15	15	15	15
DX-ZnO	15	15	7.5	15
DX-CuO	15	15	7.5	15
CuO NPs	0.625	0.625	1.25	1.25
ZnO NPs	0.23	0.47	3.75	7.5

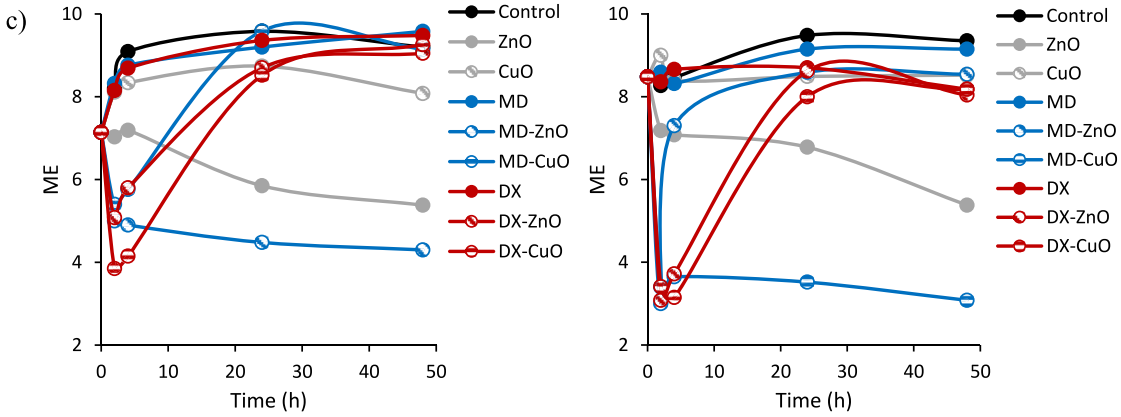

Fig. 6. a) Zinc or copper released from the microparticles after 1, 6, and 48 h (mean ± s.d.; n = 3), b) MIC and MBC values for microparticles (MD or DX) doped with CuO or ZnO, against *E. coli* ATCC 8739 and *S. aureus* ATCC 29213, c) the time-killing curves (microbicidal effect, ME, vs time) for microparticles (MD or DX) doped with CuO or ZnO against *S. aureus* ATCC 29213 (left panel) and *E. coli* ATCC 8739 (right panel).

of action seems attributable to the capability of these nanomaterials to penetrate the bacterial cell membrane mainly formed of peptidoglycan, a polymer containing amino acids and sugars, less firm and easily cross-able. Generally, the smallest the particle size the greatest the surface/-volume ratio and the highest the antibacterial effectiveness [30,32].

3.8. *In vitro whole blood clotting*

Fig. 7 shows the haemoglobin absorbance profiles after 3 min of contact with microparticles (a), the photographs showing visible blood coagulation resulting from mixing of whole blood with microparticles (b) and SEM images of the mixture of microparticles and the whole blood.

After 3 min of microparticles contact with whole blood, the % of free haemoglobin is around 25%, and this suggests a faster clot formation. No significant difference in the absorbance values is observed when microparticles are doped with ZnO or CuO NPs, confirming that the presence of NPs does not hinder the haemostatic property of the particles. These features are confirmed by SEM images in which the aggregates are evident, suggesting the blood clotting caused by the contact with microparticles. In the images, erythrocytes (red arrows) are evident and are in all the cases entrapped and surrounded from fibrin network (yellow arrows) generated by platelet activation. Rare microparticles (green arrows) appear in the fibrin network although it is conceivable that the major part is completely hidden since they act as clotting trigger.

Although the differences are not significant, generally MD seems to favour the blood clotting, and this could be due to the hydration and the swelling properties of MD based systems that are superior to those of DX based microparticles.

This is an extremely interesting property since the bleeding, an inevitable consequence of a wound that disrupts blood vessels, could lead to delayed wound healing, infection, and necrosis.

Haemostatic activity of the microparticles could be attributed to two different processes. The first one is related to the negative surface zeta potential capable to activate the intrinsic pathway of the coagulation by the activation of X, XII factors and V factor which consequently activated V factor, prothrombin (II) and fibrinogen (I) to obtain fibrin, allowing the formation of the clot.

The second one could be related to the hydration of microparticles that instantly extracts fluids from the blood, causing the concentration of proteins, platelets, red blood cells and other blood components on the surface of the microparticles. This process conceivably assists the formation of a fibrin clot and determine the haemostatic effect regardless from the coagulation cascade [33].

3.9. *In vivo safety and efficacy*

The preclinical investigation aims at evaluating the wound repair, and this take advantage of multiple aspects, as antimicrobial, proliferation enhancement and haemostatic properties that all together contribute to heal the skin lesions. In this perspective, at first, the physiological

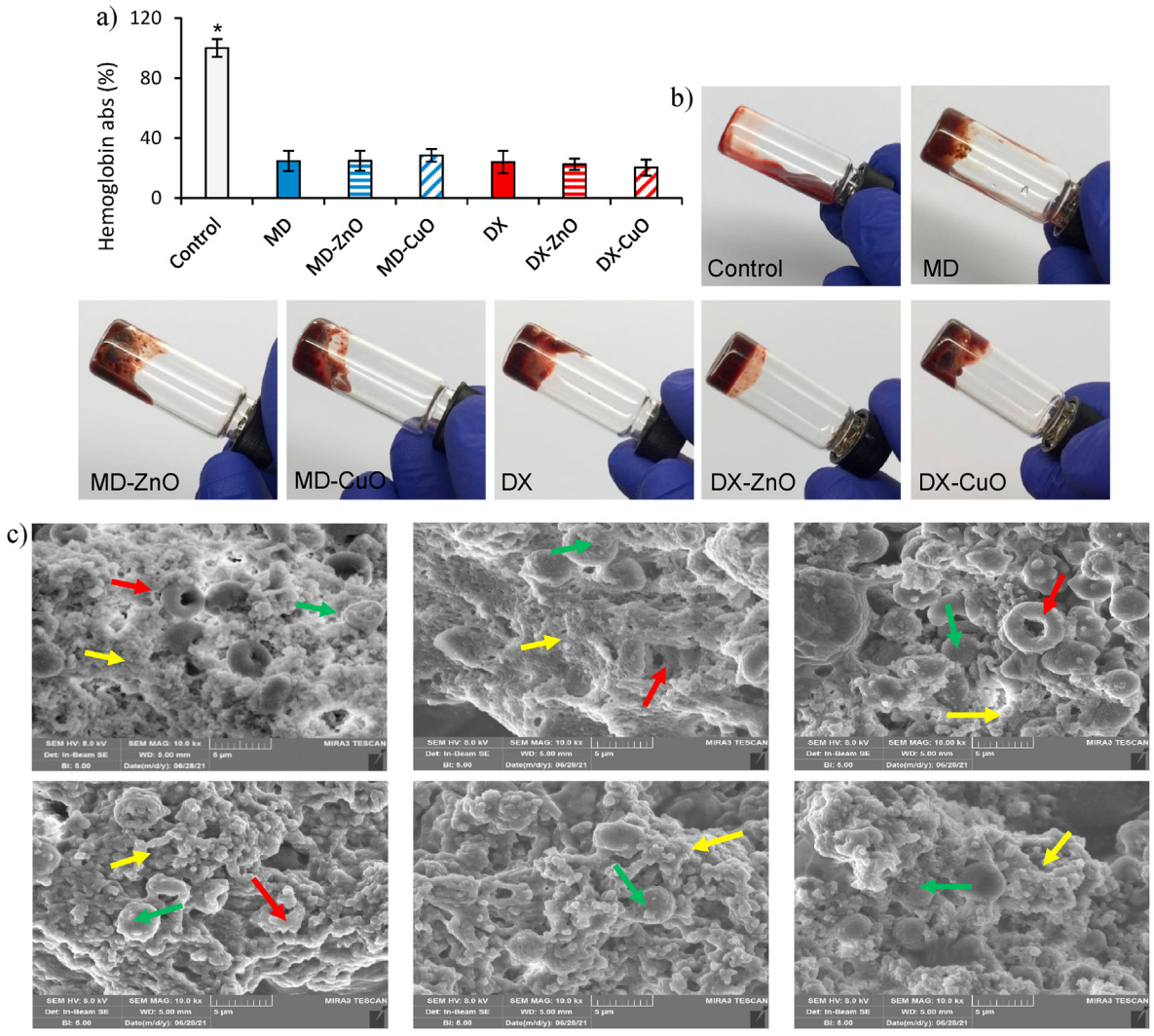

Fig. 7. a) % Haemoglobin absorbance profiles after 3 min of contact with microparticles (mean values ± sd; n = 3); b) photographs showing visible blood clotting resulting from the mixing of whole blood with microparticles; c) SEM images of the mixture of microparticles and the whole blood (erythrocytes - red arrows, fibrin network - yellow arrows, microparticles – green arrows). Values * are statistically significant ($p \leq 0.05$).

response upon implant has been evaluated to assess the systems safety. The histology analysis of wound sites after the subcutaneous and wound implants are reported in Fig. 8. Fig. S9.The histology of the tissues in correspondence of the subcutaneous implants (Fig. 8 d-i) does not show any signal of the systems and no difference is recognized from the adjacent control skin, showing not only complete regeneration of the epidermis and dermis after the surgical procedures, but also hair follicles and sebaceous glands completely restored. The epidermidis is fully restored in multiple cell layers with a fair degree of keratinization. Skin appendages (hair follicles and glands) are identical in number and disposition with respect to those of intact skin. PSR staining shows a continuous collagen layer, rich in orange-to-red fibers, with a pattern identical to that of intact skin (Fig. 8 c). In all cases, after 18 days from the implants, it is no more possible to detect microparticles or aggregates in the tissue depth. This leads to suppose that the microparticles biodegrade independently of the compositions within 18th day from the implant. This finding agrees with the in vitro degradation profiles that suggests a complete systems degradation within 10 days. The systems complete degradation in vivo should allow enhanced healing by facilitating cell migration, adhesion and proliferation into the degrading scaffolds and their replacement with native extracellular matrix. No sign of local inflammation is recognizable suggesting that the complete resorption of the structures does not cause immune response. The visual analysis of the organs after the sacrifice (data not shown) suggests that no acute toxicity signs are caused by the local treatment. Moreover, there are in literature preliminary evidence that CuO-NPs could be inherent potential toxic at higher dose levels, via oral route in rats (1000 mg/kg administered daily for 28 days) and this is due to the enhanced ROS generation [34], while ZnO NPs (250 mg/kg administered daily for 7 weeks) cause toxic effects on mice (zinc accumulation in the liver and kidney) [35]. Despite of these findings, the metal oxide doses locally administered in this work are of 1 mg/kg in a single dose and, although further investigations will be required to absolutely establish the safety profiles, these are at least 250 folds lower than the toxic ones without no repeated administrations.

To investigate the wound repair effectiveness in the healing of skin injury, the histology of the tissues in correspondence of the implants in the wound beds after the blister removal (Fig. 8 j-o) has been performed in comparison to the control lesion treated with saline solution (b) and the intact skin (c). Fig. S9 reports the representative macroscopic images of full-thickness dorsal skin wounds in the control group and the microparticles group at 0, 3, 6, 10, 13, and 17 days after injury. All the systems enhance reepithelization and accelerate collagen deposition. After 18 days of treatment, wound closure (Fig. 8 a) with a complete or almost complete epidermidis regeneration is assessable. All the histological analysis evidence an efficient remodelling of collagen fibers in orderly pattern for all the samples while the control lesion treated with

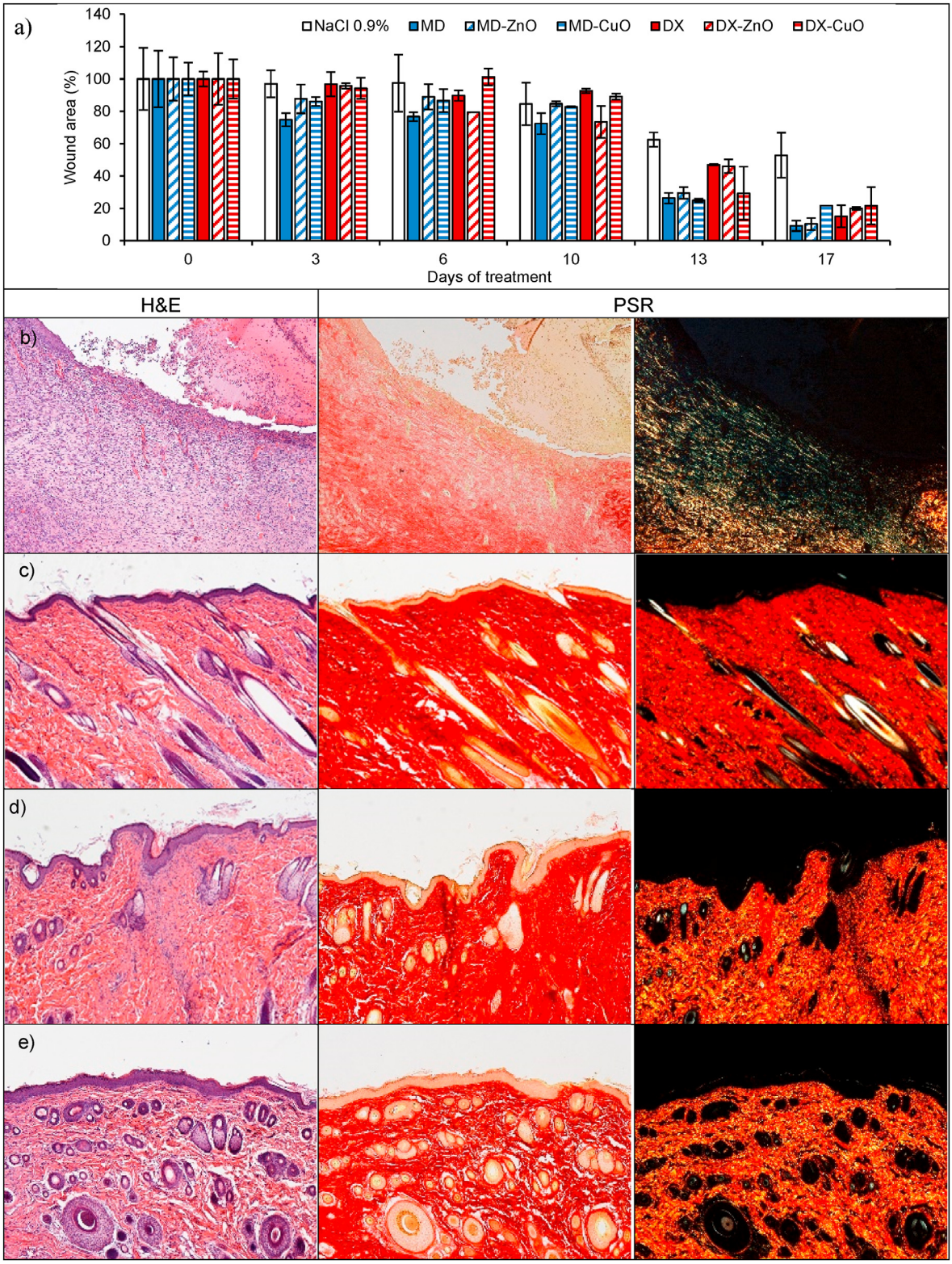

Fig. 8. a) Lesion area vs. time obtained during the treatments using microparticles and saline solution (negative control) in an in vivo murine burn/excisional model (mean values ± sd; n = 3) and H&E (left panel) and PSR (central panel - with bright-field images; right panel - with polarized light) sections of (b) lesion treated with saline solution as negative control (n = 9), (c) intact skin (n = 3), (d) subcutaneous implant of MD microparticles (n = 3), (e) subcutaneous implant of MD-ZnO microparticles (n = 3), (f) subcutaneous implant of MD-CuO microparticles (n = 3), (g) subcutaneous implant of DX microparticles (n = 3), (h) subcutaneous implant of DX-ZnO microparticles (n = 3), (i) subcutaneous implant of DX-CuO microparticles (n = 3), (j) lesion treated with MD microparticles (n = 3), (k) lesion treated with MD-ZnO microparticles (n = 3), (l) lesion treated with MD-CuO microparticles (n = 3), (m) lesion treated with DX microparticles (n = 3), (n) lesion treated with DX-ZnO microparticles (n = 3), (o) lesion treated with DX-CuO microparticles (n = 3), (Original magnification: 5X. Each micrograph frame has a width of 1780 μm); p) granulation tissue maximal length (GTML) and thickness (GTT) (μm) following the treatment with microparticles and saline solution (negative control): * indicates significative differences (mean values + sd, n = 3).

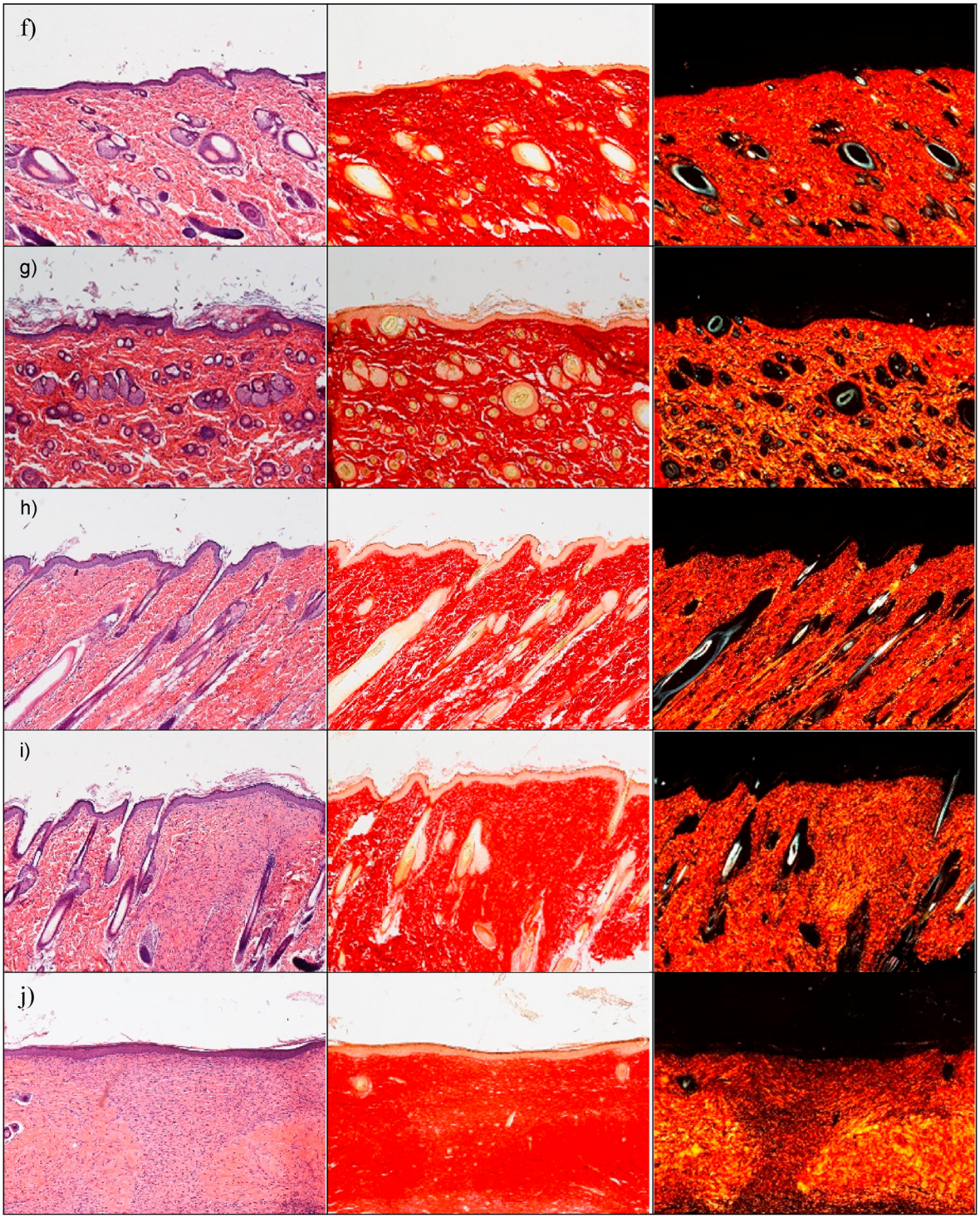

Fig. 8. (*continued*).

saline solution is not completely re-epithelialized and large amount of thin newly formed fibers is evident.

Lesions treated with MD (j), MD- ZnO (k), DX (m), DX-ZnO (n), and DX-CuO (o) show the epidermis completely restores in multiple cell layers with a fair degree of keratinization, loosely arranged collagen fibers in the underlying dermis, along with zones of normal collagen tissue. Collagen is deposited and remodelled in an appropriated orientation to withstand the tensile stresses placed on the area of repair, suggesting a maturation of the tissue. The lesions show well-formed keratinized squamous epithelium with areas of normal collagen in the underlying dermis along with few patches of loosely arranged collagen fibers surrounding hair follicles. PSR stain shows a continuous collagen layer, rich in orange-to-red fibers for all the systems. The granulation tissue created and modified by fibroblasts serves as a bed for tissue repair. Initially, it consists of a network of collagen III, a weaker form of collagen produced rapidly. This is later replaced by the stronger, long-stranded type I collagen, as evidenced in scar tissue. Formation and contraction of the granulation tissue represent integral aspects of the healing wound. The granulation process can be quantified measuring granulation tissue thickness and maximal length (Fig. 8 p).

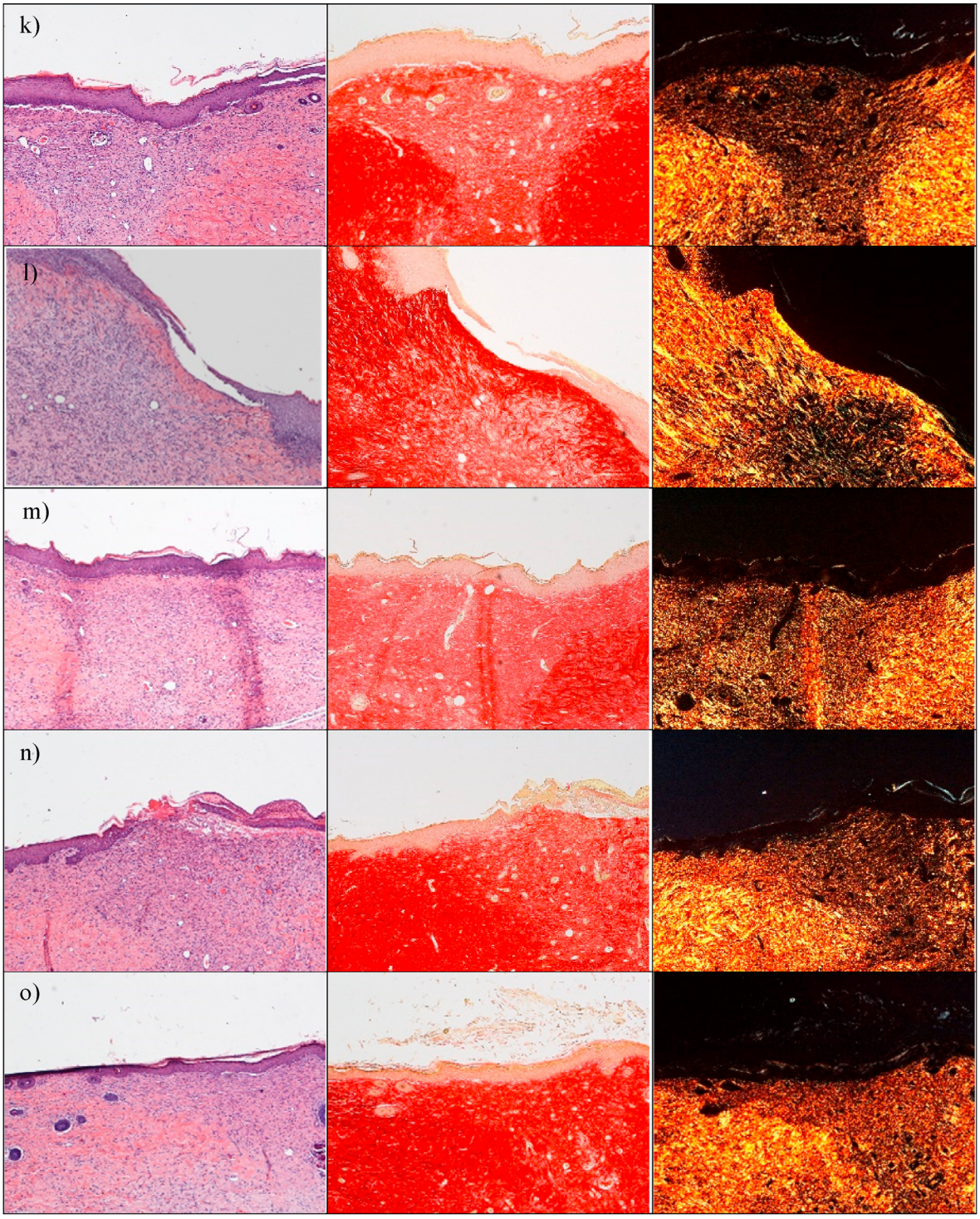

Fig. 8. (*continued*).

MD-CuO microparticles (Fig. 8 l) still determine signs of the proliferative phase of healing, with a number of blood vessels and a residual area of granulation tissue (a mixture of proliferating capillaries, fibroblasts and inflammatory cells in a loose oedematous extracellular matrix), suggesting a slightly delayed remodelling process in comparison with other treatments. Moreover, the epidermal layer is still not complete and a numerous congested blood vessels (angiogenesis) are evident. The remaining lesion is filled with highly cellular granulation tissue. PSR stain shows a large amount of orange to red birefringence in zone with accumulation of maturated thick collagen fibers. However, almost the entire surface of the lesion treated with the dressing is covered with new epithelium. In all the cases (except the tissue treated with MD-CuO) the reconstituted epithelium is completely normal and no signs of either fibrosis (collagen distributed in bundles is identical to the healthy/intact skin) or inflammation (there is no accumulation of macrophages, lymphocytes or granulocytes) is evident.

The presence of ZnO in the systems allows to have the smaller granulation tissue in the lesions indicating that the healing process

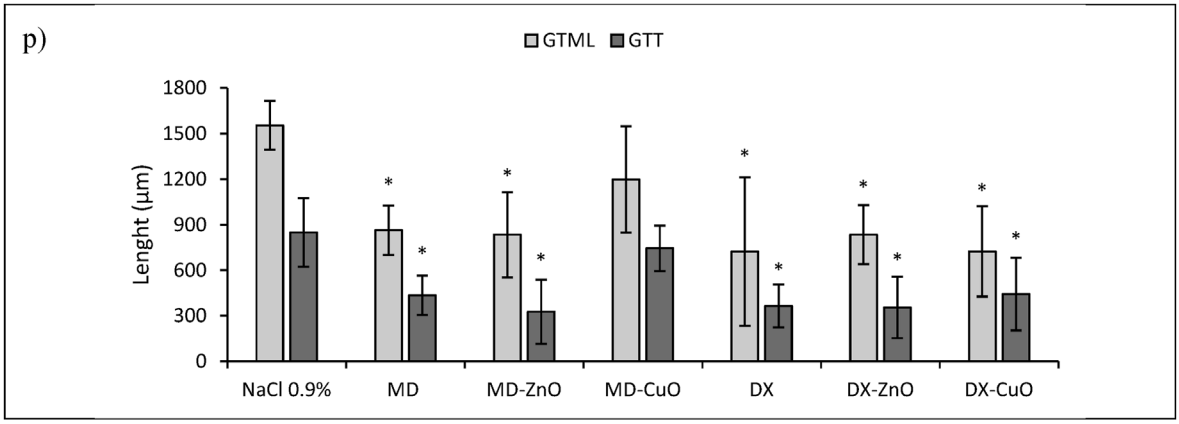

Fig. 8. (*continued*).

proceeds faster and more effectively that those in the tissue treated with CuO or undoped formulations and dextran seems to better enhance healing process.

4. Conclusions

Smart nano-in-microparticles doped with metal oxides, either ZnO or CuO, are manufactured using spray drying. Maltodextrin or dextran, respectively a linear or branched glucose polymers, are blended with amino acids (glycine, serine and threonine) to enhance wound healing. A 3D hierarchical structure is obtained. The microparticles present a spherical shape not altered by the doping and the cross-linking process by heating. This allows to obtain a more packed structure with maltodextrin, having a linear structure, rather than a looser one with the branched dextran. This is agreement with the structural analysis. The thermal behaviour suggests that the systems are stable during the cross-linking process and moreover this further enhances the systems stability upon heating. Moreover nano-in microparticles doped with ZnO or CuO are characterized by good biocompatibility towards fibroblasts although they possess the capability to avoid bacteria proliferation due to the control release of Zn or Cu having intrinsic antimicrobial properties. The negative surface zeta potentials and the hydration properties seem crucial for the proved haemostatic properties of the systems. Finally, the nano-in microparticles are safe and effective as the in vivo preclinical murine investigation proves. In particular, Cu doping delays the healing process compared to the Zn doped systems. Moreover, dextran shows superior properties from both physico-chemical and biopharmaceutical points of view. This is probably due to the 3D loser microparticle structure due to the branched polysaccharide chains that could allow a higher interaction of the polymer with the other components of the microparticles and the external environment also upon application. In conclusion, dextran based microparticles doped with ZnO deserve particular attention and further investigation will promote the prototype translation to clinics.

Author contributions

Conceptualization: G.S., M.R.; Data curation: M.R.; Formal analysis: M.R.; Funding acquisition: G.S.; Investigation: M.R.; D.C.; C.B.; A.I.C.; E.D.F.; R.S.; N.M.; J.R.; L.C.; Methodology: M.R.; Project administration: G.S.; Resources: G.S; L.C.; N.M.; C.V.; Supervision: G.S.; Visualization: M.R.; B.V; S.R; Roles/Writing - original draft: M.R.; G.S.; Writing - review & editing: M.R.; G.S; E.D.F; L.C.

Declaration of competing interest

The authors declare that they have no known competing financial interests or personal relationships that could have appeared to influence the work reported in this paper.

Acknowledgements

Authors thank Horizon 2020 Research and Innovation Programme under Grant Agreement No. 814607 for funding the research project, ESRF for financial support and beamtime (DOI: 10.15151/ESRF-ES-585935736) and ID02 staff for technical support, and the animal facility “Centro di servizio per la gestione unificata delle attività di stabulazione e di radiobiologia” of the University of Pavia (Italy) to host the animals and the OPBA of the University of Pavia for support in animal protocol drawing up.

This work benefited from the use of the SasView application, originally developed under NSF Award DMR-0520547. SasView also contains code developed with funding from the EC Horizon 2020 program under the SINE2020 project grant No 654000.

The authors wish to thank Dr. Dario Bozzo (Alfatest, Cernusco sul Naviglio, Italy) for SEM-EDX analysis.

Appendix A. Supplementary data

Supplementary data to this article can be found online at https://doi.org/10.1016/j.mtbio.2022.100418.

References

[1] S. Enoch, D.J. Leaper, Basic science of wound healing, Surgery 28 (2008) 31–37, https://doi.org/10.1016/j.mpsur.2007.11.005.

[2] M. Ruggeri, E. Bianchi, S. Rossi, C. Boselli, A.I. Cornaglia, L. Malavasi, R. Carzino, G. Suarato, R. Sánchez-Espejo, A. Athanassiou, C. Viseras, F. Ferrari, G. Sandri, Maltodextrin-amino acids electrospun scaffolds cross-linked with Maillard reaction for skin tissue engineering, Mater. Sci. Eng. C 112593 (2021), https://doi.org/10.1016/j.msec.2021.

[3] M.A. Mofazzal Jahromi, P. Sahandi Zangabad, S.M. Moosavi Basri, K. Sahandi Zangabad, A. Ghamarypour, A.R. Aref, M. Karimi, H.R. Hamblin, Nanomedicine and advanced technologies for burns: preventing infection and facilitating wound healing, Adv. Drug Deliv. Rev. 123 (2018) 33–64, https://doi.org/10.1016/j.addr.2017.08.001.

[4] F. Garcia-Villen, A. Faccendini, C. Aguzzi, P. Cerezo, M.C. Bonferoni, S. Rossi, P. Grisoli, M. Ruggeri, F. Ferrari, G. Sandri, C. Viseras, Montmorillonite-norfloxacin nanocomposite intended for healing of infected wounds, Int. J. Nanomed. 14 (2019) 5051–5060, https://doi.org/10.2147/IJN.S208713.

[5] A. Faccendini, M. Ruggeri, D. Miele, S. Rossi, M.C. Bonferoni, C. Aguzzi, P. Grisoli, C. Viseras, B. Vigani, G. Sandri, F. Ferrari F, Norfloxacin-Loaded electrospun scaffolds: montmorillonite nanocomposite vs, Free Drug. Pharmaceutics 12 (2020) 325, https://doi.org/10.3390/pharmaceutics1204032.

[6] M. Ruggeri, E. Bianchi, S. Rossi, B. Vigani, M.C. Bonferoni, C. Caramella, G. Sandri, F. Ferrari, Nanotechnology-based medical devices for the treatment of chronic skin lesions: from research to the clinic, Pharmaceutics 12 (2020) 815, https://doi.org/10.3390/pharmaceutics12090815.

[7] F. Berini, V. Orlandi, R. Gornati, G. Bernardini, F. Marinelli, Nanoantibiotics to fight multidrug resistant infections by Gram-positive bacteria: hope or reality?

Biotechnol. Adv. 57 (2022), 107948 https://doi.org/10.1016/j.biotechadv.2022.107948.
[8] A. Cassini, L.D. Hogberg, D. Plachouras, A. Quattrocchi, A. Hoxha, G.S. Simonsen, M. Colomb-Cotinat, M.E. Kretzschmar, B. Devleesschauwer, M. Cecchini, D.A. Ouakrim, Cravo T. Oliveira, M.J. Struelens, C. Suetens, D.L. Monnet, The Burden of AMR Collaborative Group, Attributable deaths and disability-adjusted life-years caused by infections with antibiotic-resistant bacteria in the EU and the European Economic Area in 2015: a population-level modelling analysis, Lancet Infect. Dis. 1 (2019) 56–66, https://doi.org/10.1016/S1473-3099(18)30605-4, 2019.
[9] K. Kalantari, E. Mostafavi, A.M. Afifi, Z. Izadiyan, H. Jahangirian, R. Rafiee-Moghaddam, T.J. Webster, Wound dressings functionalized with silver nanoparticles: promises and pitfalls, Nanoscale 12 (2020) 2268–2291, https://doi.org/10.1039/C9NR08234D.
[10] M. Godoy-Gallardo, U. Eckhard, L.M. Delgado, Y.J.D. de Roo Puente, M. Hoyos-Nogués, F.J. Gil, R.A. Perez, Antibacterial approaches in tissue engineering using metal ions and nanoparticles: from mechanisms to applications, Bioact. Mater. 6 (2021) 4470–4490, https://doi.org/10.1016/j.bioactmat.2021.04.033.
[11] M.P. Ribeiro, P.I. Morgado, S.P. Miguel, P. Coutinho, I.J. Correia, Dextran-based hydrogel containing chitosan microparticles loaded with growth factors to be used in wound healing, Mater. Sci. Eng. C 33 (2013) 2958–2966, https://doi.org/10.1016/j.msec.2013.03.025.
[12] M.A. Anwar, A.I. Aqib, K. Ashfaq, F. Deeba, M.K. Khan, S.R. Khan, I. Muzammil, M. Shoaib, M.A. Naseer, T. Riaz, Q. Tanveer, M. Sadiq, F.L. Lodhi, F. Ashraf, Antimicrobial resistance modulation of MDR E. coli by antibiotic coated ZnO nanoparticles, Microb. Pathog. 148 (2020), 104450, https://doi.org/10.1016/j.micpath.2020.104450.
[13] Y.H. Hsueh, P.H. Tsai, K.S. Lin, pH-dependent antimicrobial properties of copper oxide nanoparticles in Staphylococcus aureus, Int. J. Mol. Sci. 18 (2017) 793, https://doi.org/10.3390/ijms18040793.
[14] A.T. Iacob, M. Drăgan, O.M. Ionescu, L. Profire, A. Ficai, E. Andronescu, L.G. Confederat, D. Lupaşcu, D, An overview of biopolymeric electrospun nanofibers based on polysaccharides for wound healing management, Pharmaceutics 12 (2020) 983, https://doi.org/10.3390/pharmaceutics12100983.
[15] H. Hao, F.J. Xu, Rational design and latest advances of polysaccharide-based hydrogels for wound healing, Biomater. Sci. 8 (2020) 2084–2101, https://doi.org/10.1039/D0BM00055H.
[16] S.Y. Hung, J.S. Tsai, J.T. Yeh, K.H. Chen, C.N. Lin, H.M. Yang, C.W. Lin, H.Y. Chen, C.H. Huang, Y.Y. Huang, Amino acids and wound healing in people with limb-threatening diabetic foot ulcers, J. Diabet. Complicat. 33 (2019), 107403, https://doi.org/10.1016/j.jdiacomp.2019.06.008.
[17] A. Meduri, P.L. Grenga, L. Scorolli, P. Ceruti, G. Ferreri, Role of cysteine in corneal wound healing after photorefractive keratectomy, Ophthalmic Res. 41 (2009) 76–82, https://doi.org/10.1159/000187623.
[18] K. Amin, J. Li, W.R. Chao, M.W. Dewhirst, Z.A. Haroon, Dietary glycine inhibits angiogenesis during wound healing and tumor growth, Cancer Biol. Ther. 2 (2003) 173–178, https://doi.org/10.4161/cbt.2.2.280, https://doi.org/10.4161/cbt.2.2.280.
[19] K. Pal, A.K. Banthia, D.K. Majumdar, Polyvinyl alcohol-glycine composite membranes: preparation, characterization, drug release and cytocompatibility studies, Biomed. Mater. 1 (2006) 49–55. https://iopscience.iop.org/article/10.1088/1748-6041/1/2/001.
[20] N. Castro, V. Durrieu, C. Raynaud, A. Rouilly, Influence of DE-value on the physicochemical properties of maltodextrin for melt extrusion processes, Carbohydr. Polym. 144 (2016) 464–473, https://doi.org/10.1016/j.carbpol.2016.03.004, 2016.
[21] M. Doucet, C. Jae Hie, A. Gervaise, J. Bakker, W, Bouwman, P. Butler, K. Campbell, M. Gonzales, M. Heenan, J. Richard, A. Jackson, P. Juhas, S. King, P. Kienzle, J. Krzywon, Jeff; A. Markvardsen, T. Nielsen, L. O'Driscoll, W. Potrzebowski, R. Ferraz Leal, T. Richter, P. Rozycko, T. Snow, A. Washington. SasView Version 4.2.1 http://doi.org/10.5281/zenodo.2561236.
[22] P. Lidner, T. Zemb Neutrons, X-Rays and Light: Scattering Methods Applied to Soft Condensed Matter, first ed., North-Holland, Amsterdam, 2002.
[23] E. Gavini, G. Rassu, C. Muzzarelli, M. Cossu, P. Giunchedi, Spray-dried microspheres based on methylpyrrolidinone chitosan as new carrier for nasal administration of metoclopramide, Eur. J. Pharm. Biopharm. (2008) 245–252. https://europepmc.org/article/med/17574825.
[24] A. Nishiguchi, F. Sasaki, H. Maeda, M. Kabayama, A. Ido, T. Taguchi, Multifunctional hydrophobized microparticles for accelerated wound healing after endoscopic submucosal dissection, Small 15 (2019), e1901566, https://doi.org/10.1002/smll.201901566.
[25] C. Gavory, R. Abderrahmen, J.P. Valour, D. Chaussy, M.N. Belgacem, H. Fessi, S. Briançon, Encapsulation of a pressure-sensitive adhesive by spray-drying: microparticles preparation and evaluation of their crushing strength, J. Microencapsul. 29 (2012) 185–193, https://doi.org/10.3109/02652048.2011.642014.
[26] M. Budai-Szűcs, M. Ruggeri, A. Faccendini, A. Léber, S. Rossi, G. Varga, M.C. Bonferoni, P. Vályi, K. Burián, E. Csányi, G. Sandri, F. Ferrari, Electrospun scaffolds in periodontal wound healing, Polymers 13 (2021) 307, https://doi.org/10.3390/polym13020307.
[27] CLSI Clinical and Laboratory Standards Institute (CLSI), Performance Standards for Antimicrobial Susceptibility Testing, 28th ed., Clin. Lab. Stand. Inst., Wayne, PA, USA, 2018. CLSI Supplement M100.
[28] F. Saporito, G. Sandri, S. Rossi, M.C. Bonferoni, F. Riva, L. Malavasi, C. Caramella, F. Ferrari, Freeze dried chitosan acetate dressings with glycosaminoglycans and traxenamic acid, Carbohydr. Polym. 15 (2018) 408–417, https://doi.org/10.1016/j.carbpol.2017.12.066.
[29] U. Klinkesorn, P. Sophanodora, P. Chinachoti, E.A. Decker, D.J. McClements, Characterization of spray-dried tuna oil emulsified in two-layered interfacial membranes prepared using electrostatic layer-by-layer deposition, Food Res. Int. 39 (2006) 449–457, https://doi.org/10.1016/j.foodres.2005.09.008.
[30] K. Steffy, G. Shanthi, A.S. Maroky, S. Selvakumar, Enhanced antibacterial effects of green synthesized ZnO NPs using Aristolochia indica against Multi-drug resistant bacterial pathogens from Diabetic Foot Ulcer, J Infect Public Health 11 (2018) 463–471, https://doi.org/10.1016/j.jiph.2017.10.006.
[31] R. Rajamma, S. Gopalakrishnan Nair, F. Abdul Khadar, B. Baskaran, Antibacterial and anticancer activity of biosynthesised CuO nanoparticles, IET Nanobiotechnol. 14 (2020) 833–838, https://doi.org/10.1049/iet-nbt.2020.0088.
[32] O. Oprea, E. Andronescu, D. Ficai, A. Ficai, F.N. Oktar, M. Yetmez, ZnO applications and challenges, Curr. Org. Chem. 18 (2014) 192–203, https://doi.org/10.2174/1385272813176660143.
[33] X. Yang X, W. Liu, N. Li, M. Wang, B. Liang, I. Ullah, A. Luis Neve, Y. Feng, H. Chen, C. Shi, Design and development of polysaccharide hemostatic materials and their hemostatic mechanism, Biomater. Sci. 12 (2017) 2357–2368, https://doi.org/10.1039/C7BM00554G.
[34] L.S.P. Bugata, P. Pitta Venkata, A.R. Gundu, R. Mohammed Fazlur, U.A. Reddy, J.M. Kumar, V.R. Mekala, S. Bojja, M. Mahboob, Acute and subacute oral toxicity of copper oxide nanoparticles in female albino Wistar rats, J. Appl. Toxicol. 39 (2019) 702–716, https://doi.org/10.1002/jat.3760.
[35] C. Wang, K. Cheng, L. Zhou, J. He, X. Zheng, L. Zhang, X. Zhong, T. Wang, Evaluation of long-term toxicity of oral zinc oxide nanoparticles and zinc sulfate in mice, Biol. Trace Elem. Res. 178 (2017) 276–282, https://doi.org/10.1007/s12011-017-0934-1.